SAND2000-1657J

Mixing of Isotactic and Syndiotactic Polypropylenes in the Melt

RECEIVED
AUG 17 2000
OSTI

Thomas C. Clancy[a], Mathias Pütz[b], Jeffrey D. Weinhold[b],

John G. Curro[b*], and Wayne L. Mattice[a*]

[a] Institute of Polymer Science, The University of Akron, Akron, Ohio

[b] Advanced Materials Laboratory, Sandia National Laboratories, Albuquerque, New Mexico.

[b] This work was supported by the United States Department of Energy under Contract DE-AC04-94AL85000. Sandia is a multiprogram laboratory operated by Sandia Corporation, a Lockheed Martin Company, for the United States Department of Energy.

DISCLAIMER

This report was prepared as an account of work sponsored by an agency of the United States Government. Neither the United States Government nor any agency thereof, nor any of their employees, make any warranty, express or implied, or assumes any legal liability or responsibility for the accuracy, completeness, or usefulness of any information, apparatus, product, or process disclosed, or represents that its use would not infringe privately owned rights. Reference herein to any specific commercial product, process, or service by trade name, trademark, manufacturer, or otherwise does not necessarily constitute or imply its endorsement, recommendation, or favoring by the United States Government or any agency thereof. The views and opinions of authors expressed herein do not necessarily state or reflect those of the United States Government or any agency thereof.

DISCLAIMER

Portions of this document may be illegible in electronic image products. Images are produced from the best available original document.

Abstract: The miscibility of polypropylene (PP) melts in which the chains differ only in stereochemical composition has been investigated by two different procedures. One approach used detailed local information from a Monte Carlo simulation of a single chain, and the other approach takes this information from a rotational isomeric state model devised decades ago, for another purpose. The first approach uses PRISM theory to deduce the intermolecular packing in the polymer blend, while the second approach uses a Monte Carlo simulation of a coarse-grained representation of independent chains, expressed on a high-coordination lattice. Both approaches find a positive energy change upon mixing isotactic PP (iPP) and syndiotactic polypropylene (sPP) chains in the melt. This conclusion is qualitatively consistent with observations published recently by Mülhaupt and coworkers. The size of the energy chain on mixing is smaller in the MC/PRISM approach than in the RIS/MC simulation, with the smaller energy change being in better agreement with the experiment. The RIS/MC simulation finds no demixing for iPP and atactic polypropylene (aPP) in the melt, consistent with several experimental observations in the literature. The demixing of the iPP/sPP blend may arise from attractive interactions in the sPP melt that are disrupted when the sPP chains are diluted with aPP or iPP chains.

Introduction

Subtle effects often control the miscibility of polymer melts, sometimes with surprising results. This phenomenon is illustrated by numerous pairs of polymeric hydrocarbons, where the line between mixing and demixing is often sensitive to minor changes in covalent structure. In polypropylene (PP) melts, indirect measurements show that changes in melt miscibility can be produced by simply altering the stereochemical composition of the chains.[1-4]

Rationalization of the mechanism by which such subtle changes in detailed atomistic structure alter the miscibility is a major challenge for simulation and theory. The most accurate approach to modeling polymer melts and blends is through Monte Carlo (MC) or Molecular Dynamics (MD) computer simulations. These simulation methods give formally exact results, but are very computationally demanding, since one needs to treat a relatively large size system consisting of many chains of high molecular weight, at liquid-like densities. Chains with a high degree of polymerization are often need for observation of demixing in experiment. This consideration implies the necessity for a theory or simulation that can treat large distance and time scales. The calculation must achieve a full equilibration, even when the driving force for immiscibility (when it exists) is subtle, as must be the case in the PP melts, where all monomer units have the same atomic composition, C_3H_8. Coarse-grained models supply the necessary distance and time scales. On the other hand, the models must accurately incorporate atomistic details, since it is the consequences of minor changes in those details that is of interest. In the PP melts, the chains must not only know that they are polypropylene; they must also accurately reflect the properties of a polypropylene of a specific stereochemical composition.

We have independently developed different methods that can qualitatively reproduce the observation by Mülhaupt and coworkers that isotactic polypropylene (iPP) and syndiotactic polypropylene (sPP) are immiscible in the melt.[2-4] The two methods share the features of incorporating information at the level of atomistic detail using well-known simulation methods. They then process this information in a very different manner in order to obtain predictions for

the behavior of the mixtures. One method takes the detailed local information from a MC simulation on a single chain, and then uses PRISM theory to deduce intermolecular packing in the polymer melt or blend.[5,6] The other method incorporates the local information from a rotational isomeric state (RIS) model for the polymer, and then employs a MC simulation on a high coordination lattice to investigate the miscibility.[7,8] Here we describe separately the application of both approaches to PP melts, focusing both on the structure of the melts and the energy changes on mixing. Then we compare the current status of the two methods.

Polypropylene Melts from the Viewpoint of PRISM Theory

Method

Polymer RISM or PRISM theory was developed by Curro and Schweizer[9-11] as an extension to polymers of the reference interaction site model of Chandler and Andersen.[12,13] Since it has been extensively discussed in previous publications,[5,6] here we will only briefly summarize the theory. Since the theory is based on liquid state physics concepts, its output is information about the structure of the polymer melt or blend as expressed through a set of pair correlation functions. Once having the structure of the liquid, most thermodynamic properties, such as the solubility parameter of a melt, or the heat of mixing of a blend, can be inferred.

We consider a united atom model for PP in which the monomeric structure is represented by overlapping, spherically-symmetric sites as shown in Figure 1. As can be seen from this figure, the hydrogen atoms are absorbed into the three independent sites designated A, B, and C corresponding to the CH_2, CH, and CH_3 moieties, respectively. Furthermore, we employ the bond length, bond angle, and rotational potentials proposed recently by Martin and Siepmann[14] and used previously by Pütz and coworkers[15] to model iPP and sPP melts with PRISM theory and MD simulation. The stereochemical structure corresponding to the isotactic and syndiotactic isomers is also preserved.

The intermolecular packing in the polymer melt or blend is characterized by the intermolecular radial distribution functions $g_{\alpha\gamma}(r)$ between sites of type α or γ on different polymer chains. One starts by writing the generalized Ornstein-Zernike equation[5,6]

$$\hat{\underline{h}}(k) = \hat{\underline{\Omega}}(k) \cdot \hat{\underline{C}}(k) \cdot \left[\hat{\underline{\Omega}}(k) + \rho \hat{\underline{h}}(k) \right] \qquad (1)$$

that relates the intermolecular packing $h_{\alpha\gamma}(r) = g_{\alpha\gamma}(r) - 1$ to the average intramolecular structure characterized by the matrix $\hat{\underline{\Omega}}(k)$.

$$\hat{\Omega}_{\alpha\gamma}(k) = \frac{1}{N_\alpha} \sum_{i\in\alpha} \sum_{j\in\gamma} \left\langle \frac{\sin kr_{ij}}{kr_{ij}} \right\rangle \qquad (2)$$

The indices i and j sum over the sites of type α and γ on a single chain. In equations 1 and 2, and throughout this paper, a caret above a variable denotes the Fourier transform with respect to the wave vector k. $\underline{C}(r)$ is the matrix of direct correlation functions $C_{\alpha\gamma}(r)$ between intermolecular sites.

Following conventional liquid state arguments[5,6,16] the direct correlation function plays the role of a renormalized pair potential that approximately accounts for many body correlations. For van der Waals interactions at liquidlike densities $C_{\alpha\gamma}(r)$ is a short range function of r and can be well approximated by the Percus-Yevick closure relation[5,6,16]

$$C_{\alpha\gamma}(r) = \left\{1 - \exp\left[\beta v_{\alpha\gamma}(r)\right]\right\} g_{\alpha\gamma}(r) \qquad (3)$$

where $v_{\alpha\gamma}(r)$ is the united atom potential between intermolecular sites that we take to have the Lennard-Jones (LJ) form.

$$v_{\alpha\gamma}(r) = 4\varepsilon_{\alpha\gamma}\left[\left(\frac{\sigma_{\alpha\gamma}}{r}\right)^{12} - \left(\frac{\sigma_{\alpha\gamma}}{r}\right)^{6}\right] \qquad (4)$$

It is well established[5,6,17,18] that at liquidlike densities, the liquid structure is dominated by the repulsive part of the potential. Attractions are very important in determining the thermodynamic

properties but do not significantly affect the intermolecular pair correlations. This fact leads us to decompose the LJ potential of equation 4 into a repulsive part v_r and an attractive part v_a. Following Weeks, Chandler and Andersen[19] we employ

$$v_r(r) = 4\varepsilon\left[\left(\frac{\sigma}{r}\right)^{12} - \left(\frac{\sigma}{r}\right)^{6} + \frac{1}{4}\right] \qquad r \le 2^{1/6}\sigma$$

$$v_r(r) = 0 \qquad r \ge 2^{1/6}\sigma \tag{5a}$$

for the repulsive branch and

$$v_a(r) = -\varepsilon \qquad r \le 2^{1/6}\sigma$$

$$v_a(r) = 4\varepsilon\left[\left(\frac{\sigma}{r}\right)^{12} - \left(\frac{\sigma}{r}\right)^{6}\right] \qquad r \ge 2^{1/6}\sigma \tag{5b}$$

for the attractive or perturbative part of the LJ potential. Previous experience[5,6] has demonstrated that PRISM theory gives the most accurate results for the melt structure if only the repulsive branch of the potential is used. In this investigation we used the WCA repulsive potential from equation 5a in the PY closure given in equation 3.

Equations 1 and 3 provide a relationship between the inter and intramolecular structure of a polymer melt or blend. Thus if we are able to compute the average intramolecular structure in equation 2, we then can obtain the intermolecular packing by solving the integral equations in equations1 and 3. The solution of these coupled integral equations can be obtained numerically[5,6,20] by using standard Picard iteration techniques. To first approximation, one can

estimate $\hat{\underline{\Omega}}(k)$ by employing the Flory ideality hypothesis[5,6,21] by assuming the excluded volume interactions are screened in the melt and the intramolecular structure is ideal. Previously, Curro and coworkers[22] applied this approach to model the packing in iPP and sPP melts by calculating the matrix $\hat{\underline{\Omega}}(k)$ from a single chain Monte Carlo simulation. In this simulation, repulsive interactions beyond sites separated by five bonds were set to zero in keeping with Flory's hypothesis. More accurate calculations, however, require us to compute both the intramolecular structure $\hat{\underline{\Omega}}(k)$ and the intermolecular packing $g_{\alpha\gamma}(r)$ in a self-consistent manner.

Self-consistent PRISM calculations[5,6] have been carried out recently on melts of polyethylene,[23] iPP, sPP, polyisobutylene,[20] as well as head-to-head PP and poly(ethylene propylene).[15] These self-consistent computations involve performing a single chain MC simulation for the polymer with all the intramolecular repulsive LJ interactions turned on. The effect of the remaining chains in the melt is approximated through an additional intramolecular "solvation potential" $W_{\alpha\gamma}(r)$ acting between all pairs of intramolecular sites. The form of this solvation potential was taken to be in Fourier space as

$$\beta \hat{\underline{W}}(k) = -\hat{\underline{C}}(k) \cdot \hat{\underline{S}}(k) \cdot \hat{\underline{C}}(k) \qquad (6)$$

where $\hat{S}_{\alpha\gamma}(k)$ is the structure factor matrix defined according to

$$\hat{S}_{\alpha\gamma}(k) = \rho_\alpha \hat{\Omega}_{\alpha\gamma}(k) + \rho_\alpha \rho_\gamma \hat{h}_{\alpha\gamma}(k) \qquad (7)$$

where ρ_α is the density of sites of type α. Near contact between sites on the same macromolecule, the solvation potential is generally attractive and serves to counterbalance the

repulsive, intramolecular, excluded-volume interactions. The essence of the Flory ideality hypothesis is that the excluded volume and solvation forces effectively cancel each other out.

It can be seen that the solvation potential in equation 6 involves both $C_{\alpha\gamma}(r)$ and $g_{\alpha\gamma}(r)$ which requires the solution of equations 1 and 3. At the same time the solution of the PRISM equations requires a knowledge of the intramolecular structure and hence the solvation potential. A self-consistent solution can be obtained by guessing $W_{\alpha\gamma}(r)$, calculating $\hat{\underline{\Omega}}(k)$ from a single chain simulation, and then solving PRISM theory in equations 1 and 3 for $C_{\alpha\gamma}(r)$ and $g_{\alpha\gamma}(r)$ resulting in a new estimate of the solvation potential. This process is repeated until $W_{\alpha\gamma}(r)$ doesn't change from one iteration to the next within some tolerance. Reasonable self-consistent solutions can usually be found after 20 – 30 iterations. Evidently it would seem that the single-chain MC simulation would need to be performed during each loop of the self-consistent calculation when a new solvation potential is introduced. Considerable computation time can be saved, however, by saving the configurations from a MC simulation performed with a suitably chosen "umbrella potential". These configurations can then be "reweighted" according to the solvation potential appropriate to each subsequent iteration.

Results for Polypropylene Melts

Recently, self-consistent PRISM calculations have been carried out on iPP and sPP melts.[15,20] In the work of Pütz and coworkers,[15] detailed comparisons were made between PRISM calculations and full MD simulations on PP melts of macromolecules of $N = 12$ monomer units. Very good agreement was seen between theory and simulation, however, PRISM theory tended to predict excessive overlapping of intermolecular sites relative to the exact MD simulation of the melt. During the course of these self-consistent PRISM calculations, the single chain structure functions defined, in equation 2, were determined for both iPP and sPP in their respective one-component melt states. In this investigation we employ these same intramolecular structure factors to the mixture of iPP and sPP at $T = 453$K. By employing these melt structure functions $\hat{\underline{\Omega}}(k)$ to the blend, we essentially assume that the average single chain structure is not significantly changing in the blend as a function of composition. We expect this to be a reasonable first approximation based on earlier MD simulations on athermal blends by Stevenson and coworkers.[24,25] They found that the mean square end-to-end distance of each component changed by less than 10% over the complete concentration range of the blend.

In the case of the one component PP melts, there are six independent intermolecular pair correlation functions: g_{AA}, g_{BB}, g_{CC}, g_{AB}, g_{AC}, g_{BC} between the various types of sites. For a blend of sPP and iPP, 21 independent functions $g_{\alpha\gamma}(r)$ are now required to completely specify the intermolecular packing. Since we are inputting the single chain structure of both iPP and sPP from the one component melt, the PRISM calculation of the blend is not done self-consistently. Straightforward Picard iteration of equations 1 and 3 generally leads to a solution for the 21 intermolecular $g_{\alpha\gamma}(r)$ functions for the blend as a function of the composition.

In order to determine the PRISM equations in equation 1 it is necessary to know how the density changes with composition at fixed pressure. In principle this can be accomplished[26] by computing the partial molar volumes of each component as a function of composition through

the Kirkwood-Buff relations.[27] For computational convenience, we will assume that the volume change on mixing is zero in the present investigation. This implies that the density of the mixture $\rho(x)$ is given by

$$\frac{1}{\rho(x)} = \frac{x}{\rho^0_{iPP}} + \frac{1-x}{\rho^0_{sPP}} \qquad (8)$$

where x is the mole fraction of iPP monomers and $\rho^0_{iPP} = 0.010905$ Å^{-3}, $\rho^0_{sPP} = 0.010939$ Å^{-3} are the monomer densities of iPP and sPP melts at 453K.

We employ the PY closure of equation 3 with the WCA repulsive potential of equations 5a.. The same LJ parameters[14] that were used in the pure component melt calculations were used in the blend: $\sigma_{AA} = 3.95$ Å, $\varepsilon_{AA}/k_B = 46$K; $\sigma_{BB} = 4.68$ Å, $\varepsilon_{BB}/k_B = 10$K; and $\sigma_{CC} = 3.75$ Å, $\varepsilon_{CC}/k_B = 98$K for both iPP and sPP. The cross terms were assumed to obey Berthelot scaling:

$$\sigma_{\alpha\gamma} = \frac{1}{2}\left(\sigma_{\alpha\alpha} + \sigma_{\gamma\gamma}\right) \qquad \varepsilon_{\alpha\gamma} = \sqrt{\varepsilon_{\alpha\alpha}\varepsilon_{\gamma\gamma}} \qquad (9)$$

The average radial distribution functions of iPP and sPP in the 50/50 blend are shown in Figure 2 along with the results for the pure component liquids. As can be seen in the figure, the packing in the blend is very similar to the pure component packing in the melts for both iPP and sPP for these short chains of 12 monomers. Nor surprisingly, the average over the 9 cross iPP/sPP pair correlation functions falls midway between as can be seen as the dashed line in Figure 2. Thus for this short chain system, the average intermolecular packing in the blend is very similar to the melt.

Much more detail regarding chain packing in the mixture can be obtained from the 21 individual site/site pair correlation functions. In Figure 3 we have plotted the $g(r)$ functions between sites of the same type in the blend and the one-component melts. It can be observed

that the CH_3/CH_3 correlations are strong at small distances near contact. This is to be expected since the methyl groups are on the outside of the polymer backbones and can approach each other readily in the melt or blend. Correlations between backbone sites CH or CH_2 are screened at short distances by the presence of the substituted methyl groups as can be seen in Figure 3. Again we observe that these site/site correlations in the 50/50 blend are essentially the same as in the pure component liquids. The cross terms shown by the dashed lines are correlations between a site on an iPP chain with a corresponding site on an sPP molecule.

Most of the 21 intermolecular radial distribution functions did not show any significant tendencies for preferential packing in the mixture. The only exceptions were correlations between CH and CH_2 groups with CH_3 groups. Figure 4 depicts the $g(r)$'s between CH_2 and CH_3 sites. It can be observed that the correlations for site pairs for iPP and sPP in the blend and the pure component melts are close. Note, however, that there is a slight preference for a methyl group on an iPP macromolecule to be near a methylene group on an sPP chain. At the same time there seems to be a slight aversion for a methyl on sPP to be near a methylene on iPP. Although it is not shown in the figure, qualitatively similar behavior was observed for packing of CH and CH_3 sites in the mixture.

Since there do not seem to be any strong tendencies for preferential packing in the low molecular weight iPP/sPP blend, the mixture is probably miscible. We can use the various correlation functions to estimate the solubility parameters of the one-component melts and the heat of mixing of the blend. The cohesive energy density E is related to the pair correlation functions through the relation

$$E = 2\pi \int_0^\infty \sum_{\alpha\gamma} \rho_\alpha \rho_\gamma v_{\alpha\gamma}(r) g_{\alpha\gamma}(r) r^2 dr \qquad (10)$$

where $v_{\alpha\gamma}(r)$ is the complete Lennard-Jones potential (including attractions) between sites α and γ. To good approximation we use the intermolecular radial distribution functions $g_{\alpha\gamma}(r)$ from the

PRISM solution with the WCA repulsive potentials. Equation 10 can be applied to either the pure component system or to the mixture. Using equation 10 on the one-component melts, we calculated the solubility parameters, $\delta = E^{1/2}$, of both iPP and sPP at $T = 453$K to be: $\delta_{iPP} = 5.64$ $(cal/cm^3)^{1/2}$ and $\delta_{sPP} = 5.76$ $(cal/cm^3)^{1/2}$.

The heat of mixing per monomer can be obtained from the cohesive energies of the mixture and the pure components

$$\frac{\Delta H_{mix}}{N_m k_B T} = \frac{E(x)}{\rho(x)} - \left[\frac{x E_{iPP}}{\rho^0_{iPP}} + \frac{(1-x) E_{sPP}}{\rho^0_{sPP}} \right] \qquad (11)$$

where N_m is the total number of monomers in the blend. If we assume the volume of the iPP and sPP monomers are the same, then the volume and mole fractions of iPP monomers are equal: $\phi = x$. A plot of the heat of mixing calculated from equation 11 is shown in Figure 5 as a function of composition. Note in particular that the heat of mixing is positive.

It is interesting to compare the heat of mixing obtained from equation 11 with an estimate obtained from the conventional solubility parameter analysis.[28]

$$\frac{\Delta H_{mix}}{N_m k_B T} \cong \frac{\left(\delta_{iPP} - \delta_{sPP}\right)^2}{\sqrt{\rho^0_{sPP} \rho^0_{iPP}}\, k_B T} \phi(1-\phi) \qquad (12)$$

The solubility parameter estimate is shown in Figure 5 as the dotted curve. It can be observed that for this mixture, the solubility parameter analysis gives qualitatively similar results to the more exact heat of mixing from equation 10. The estimate, however, predicts a larger heat of mixing (for $\phi = 0.5$) by over a factor of 2. The extent to which the exact result differs from the solubility parameter estimate is a measure of how much the individual pair correlation functions $g_{\alpha_i}(r)$ in the blend depend on composition. For instance, it is possible to obtain a negative heat of

mixing from equation 11 if the $g_{\alpha\gamma}(r)$ functions in the blend are composition dependent. On the other hand, the solubility parameter analysis obviously will always predict a positive heat of mixing.

The self-consistent PRISM calculations presented here are for iPP and sPP chains of only 12 monomers at $T = 453$K. One would expect that the heat of mixing would have some molecular weight and nonlinear temperature dependence. Assuming for the sake of argument that $\Delta H_{mix}/N_m k_B T$ is independent of chain length and temperature, then we could argue that the iPP/sPP blend would phase separate at sufficiently high molecular weights. Furthermore, it we assume that the entropy of mixing is given by the combinatorial entropy of mixing in the Flory-Huggins theory,[28] then we can estimate the critical degree of polymerization N^*. From the heat of mixing at $\phi = 0.5$ predicted by PRISM theory, we estimate the effective chi parameter to be $\chi \cong 3.54 \times 10^{-4}$. From this we estimate that $N^* \approx 5650$ is required for the 50/50 blend to demix.

Polypropylene Melts from the Viewpoint of RIS/MC Simulation

Method

The simulation uses a bridging technique[7] that has been devised for connecting fully atomistic and coarse-grained descriptions of dense amorphous polymers. It was developed initially for application to polyethylene melts, but has also been applied to melts of PP and poly(vinyl chloride). With the aid of the rotational isomeric state model,[29,30] an atomistic description of the system at bulk density is mapped onto a coarse-grained description, at the same density, on a sparsely occupied high coordination ($10i^2 + 2$ cells in shell i) lattice.[31] The coarse-grained model retains a single site for each C_2H_4 unit of polyethylene, or C_3H_6 unit of PP. The high coordination lattice is obtained by elimination of every second site from a diamond lattice. Since the step length on the diamond lattice represents a C–C bond, the step length on the high coordination lattice is of length 2.5 Å. The density of typical melts is obtained at low occupancy (~18% for polyethylene,[32] ~12% for PP[33]). Sparse occupancy facilitates efficient equilibration of large systems. Retention of the initial stereochemical sequence of the coarse-grained chains requires that the simulation on the high coordination lattice be performed in a manner that retains a memory of the specific diamond lattice from which it was obtained.[34] The specific site retained for each monomer unit on the coarse-grained lattice corresponds to sphere B in Figure 1.

The Hamiltonian in the Metropolis MC simulation of the coarse-grained system has two parts. There is a short-range intramolecular contribution derived from the RIS model for the atomistic description of the chains.[31,34] The intermolecular contribution is obtained from an absolute prohibition of double occupancy of any site and a continuous potential energy function for the interaction of the sets of atoms represented by a pair of beads in the coarse-grained model. Discretization of the continuous potential energy function is obtained via the Mayer f function that is employed in the description of the second virial coefficient of nonideal gases.[32]

$$B_2 = -\frac{1}{2}\left[\int_0^\infty \{\exp(-\beta v(r)) - 1\}\right] = -\frac{1}{2}\int_0^\infty f dr \qquad (13)$$

Breaking the integral over all space into contributions from consecutive shells on the high coordination lattice yields

$$B_2 = \frac{V_{cell}}{2}\left[1 - \sum_i z_i \langle f \rangle_{ith}\right] \qquad (14)$$

where the z_i are the coordination numbers, $10i^2 + 2$, and $\langle f \rangle_{ith}$ is the average of the Mayer f function over the i^{th} shell,

$$\langle f \rangle = \int_{shell} f d\mathbf{r} / \int_{shell} d\mathbf{r} \qquad (15)$$

Then the averaged Mayer f function is converted into an interaction energy for that shell via

$$\exp(-\beta v_i) - 1 = \langle f \rangle_{ith} \qquad (16)$$

Equations 15 and 16 effectively convert a continuous potential energy function, $v(r)$, into a stepwise function, v_i, for use in shell i on the high coordination lattice. When applied at 473K using the LJ parameters tabulated for propane,[35] $\varepsilon/k_B = 237.1$ K and $\sigma = 5.118$ Å, this procedure yields energies (kJ/mol) of 26.851, 3.068, -1.089, -0.464, and –0.127 for shells 1–5, respectively.

The first two shells are repulsive because, with a lattice spacing of 2.50 Å, they lie within the distance specified by σ. The major attraction is in the third shell.

Equilibrated coarse-grained replicas can be rapidly reverse-mapped, thereby restoring all of the missing bonds and atoms (including hydrogen atoms), and transforming the system from the discrete space of the high coordination lattice to continuous space.[36] The reverse-mapping employs an energy minimization that transfers the chains from the discrete space of the lattice into a nearby local energy minimum in continuous configuration space.

A prior application to the simulation of PP melts was restricted to relatively small systems (eight independent parent chains)[37] and did not achieve a complete equilibration due to a problem with the acceptance of the reptation move. Miscibility of the melt of iPP and atactic polypropylene (aPP), and immiscibilty of the melt of iPP and sPP, could be inferred from the height of the first maximum in the pair correlation functions. Here we report studies of larger systems, with 18 independent parent chains, in which the differences in miscibility are more easily detected than was the case in the earlier work. The larger systems are more completely equilibrated because of the incorporation into the simulation of additional moves that alter the positions of 2–5 consecutive beads in a chain.[38] These new moves are of great assistance in the equilibration of sPP. The new simulation also uses a refinement in the description of the intermolecular contribution to the Hamiltonian, achieved with replacement of the spherically symmetric $v(r)$ in equation 8 with a directional $v(\mathbf{r})$. This directional $v(\mathbf{r})$ results in a reduction of the energies of the second shell (3.068 kJ/mol before reduction) by ~1 kJ/mol for most orientations and an increase by ~7.5 kJ/mol for those orientations in which there is strong steric repulsion between methyl groups. These strong repulsions are in orientations in which the methyl side chains are pointed directly at each other and are in a first shell occupancy.[38] Exactly the same $v(\mathbf{r})$ was assumed for the intermolecular interaction of all pairs of beads, independent of the stereochemical composition of the chain to which they belong. The RIS model of Suter et al.[39] is the same one used in prior work. This RIS model was devised initially to assist in the

interpretation of the mixtures obtained upon epimerization to stereochemical equilibrium of oligomers of PP.

The simulations were performed at 473 K, using chains represented by fifty beads each. Reverse mapping converts each chain into $C_{150}H_{302}$, with a molecular weight of 2102. This degree of polymerization was chosen so that none of the systems would be above the entanglement molecular weight. This molecular weight has been reported to be 2170, 6900, and 7050 for sPP, aPP, and iPP, respectively.[40] The density of all of the melts is 0.750 g/cm^3, based on Orwoll's tabulation of melt densities of aPP.[41] This density is achieved with occupancy of 11.85% of the sites on the high coordination lattice. The aPP chains have Bernoullian statistics, with the probability of a meso diad being 0.5.

Results for Polypropylene Melts

Snapshots of Equilibrated Melts. Figure 6 depicts a snapshot of an equilibrated melt containing equal numbers of independent iPP and aPP chains. Substantial intermixing of the two types of chains is apparent, consistent with the experiments reported by Lohse.[1] Figure 7 depicts a snapshot of another equilibrated melt in which all of the aPP chains from Figure 1 have been replaced by sPP chains. A difference in miscibility is apparent from casual inspection of the two figures. Figure 8 depicts the result for an equilibrated 50/50 blend of aPP and sPP. Here there is also visual evidence for phase separation, although the demixing does not appear to be quite as strong as in the iPP/sPP blend in Figure 7.

No physical significance should be attributed to the "lamellae" in Figure 7; their appearance is an artifact produced by the drive for phase separation in conjunction with the periodic boundary conditions employed in the separation. It is the phase separation itself, rather than the details of the "lamellae", that is of interest.

The phase separation in the iPP/sPP system, and the stronger intermixing in the iPP/aPP system, are qualitatively consistent with the observations reported by Mülhaupt and coworkers.[2-4] However, the phase separation of the iPP/sPP system in the simulation is stronger than that observed in the experiment. At this temperature, substantially longer chains are required for observation of phase separation in the experiments than those that were used in the simulation. This result suggests that fine tuning of one or more parameters in the simulation would be required for quantitative agreement with experiment. The present set of parameters produces qualitative agreement (immiscibility increases in the series iPP/aPP, aPP/sPP, iPP/sPP), and may be sufficient to provide insight into the molecular origin of the immiscibilty.

Pair Correlation Functions. Pair correlation functions were obtained from reverse-mapped replicas of the equilibrated melts. Similar trends were observed in the pair correlation functions evaluated for the beads on the high coordination lattice and for the CH groups after reverse mapping. We focus first on the pair correlation functions evaluated using the carbon

atoms in the 50/50 melts. The data are depicted in Figures 9–11 for iPP/aPP, aPP/sPP, and iPP/sPP, respectively. Each figure has four curves. One curve is evaluated using all of the carbon atoms, two curves consider only those carbon atoms in chains of a specified stereochemical composition, and the last curve is the cross-term, evaluated using pairs of carbon atoms from chains with different stereochemical compositions. These four curves become more distinguishable from one another in the series iPP/aPP, aPP/sPP, iPP/sPP. The differences in the appearance of the three figures is not, however, caused by the pair correlation functions calculated using all of the carbon atoms, as is seen in Figure 12, which reproduces the curves labelled "Total" from Figures 9–11. Therefore the differences seen in Figures 9–11 arise from the behavior of the pair correlation functions evaluated for selected components of the mixtures.

The curve for the cross-term lies within the range specified by the other three curves for iPP/aPP, but it is definitely lower than the other three curves at 4 Å $< r <$ 12 Å in the aPP/sPP and iPP/sPP blends, with the effect being larger for iPP/sPP. This result in the pair correlation functions is consistent with miscibility for iPP/aPP and immiscibility for the other two systems, with the immiscibilty being stronger for iPP/sPP than for aPP/sPP. The numerical results in the pair correlation functions reinforce the qualitative conclusions extracted from visual inspection of Figures 6–8.

The pair correlation functions evaluated for the 50/50 iPP/sPP blend from the MC simulation of coarse-grained chains with a degree of polymerization of 50 (Figure 11) show stronger demixing than the pair correlation functions evaluated from PRISM theory and a chain with a degree of polymerization of 12 (Figure 2). Both figures find the sPP/sPP pair correlation function has higher values near $r = 6$ Å than does the iPP/iPP pair correlation function. A definite maximim in the sPP/sPP pair correlation function near $r = 6$ Å is observed in the MC simulation , but not in the PRISM calculation. In the MC simulation, the iPP/sPP pair correlation is lower than the other two correlation functions for 4 Å $< r <$ 15 Å, but with the PRISM calculation it lies between the iPP/iPP and sPP/sPP pair correlation functions.

The sPP/sPP curves in Figures 10 and 11 show evidence for two maxima, located at approximately 6 and 12 Å, a feature also seen in the intermolecular pair correlation function for the backbone carbon atoms in a recent MD simulation of the melt.[42] The second maximum is stronger in the less miscible iPP/sPP blend, Figure 11. These two maxima are also easily seen in the pair correlation function for the one-component melt of sPP, but they are less obvious in the pair correlation functions for the other one-component melts, as seen in Figure 13. These pair correlation functions suggest that the sPP melt retains more "structure" than do the melts of aPP or iPP. Other evidence, to be presented below, suggests that resistance of this "structure" to disruption by dilution with aPP or iPP may contribute to the poor miscibility of sPP with the other two polypropylenes.

Change in Energy on Mixing. The iPP and aPP melts reach steady values for the energy per monomer after a million MC steps. Discarding the first million MC steps and averaging over the final two million MC steps gives the results in the first two rows of Table 1. Larger uncertainties are seen in the aPP melt than in the iPP melt. The LJ potential contributes more to the uncertainty than does the RIS portion of the energy. The LJ contribution is negative, as must be the case if the system is cohesive. There is no special significance to the positive sign for the RIS energy; it is merely a consequence of the arbitrary choice of a reference state in the RIS model.[39]

The sPP melt reaches equilibrium more slowly than the iPP or aPP melts. Therefore two sets of results are presented for sPP in Table 1. The standard deviations become smaller, and comparable in size with those obtained for the iPP and aPP melts, if the larger portion (seven million MC steps) of the equilibration period is discarded, and the average energy is evaluated from the final two million MC steps. The sPP chains have RIS energies and LJ energies that are more negative than the values seen with iPP or aPP.

The 50/50 binary mixtures containing sPP seem to oscillate in degree of mixing/demixing, perhaps because the systems are not infinitely large. This oscillation is seen in the energy per monomer, which correlates with the pair correlation function as a function of MC

step. Averaging over the last five million MC steps of the total of ten million MC steps yields the results in Table 2. The standard deviations for the total energy and its LJ and RIS components are smallest in the iPP/aPP blend. The presence of sPP in the melt leads to larger standard deviations.

Since the RIS energy is of intramolecular origin, it can be decomposed into contributions from each of the different types of PP. When the standard deviations are taken into account, the RIS energies of the iPP (~7 kJ/mol) and aPP (~6.2–6.4 kJ/mol) are nearly same in their blend (Table 2) and in their pure melts (Table 1). This result is consistent with the notion that the chains have a similar distribution of conformations in their one-component melts and in the blends. The sPP chain, however, appears to have an RIS energy that is lower in its one-component melt (~3.9 kJ/mol, Table 1) than in its two-component melts (~ 4.6 kJ/mol, Table 2). This difference in RIS energies implies that the distribution of conformations of an sPP chain depends on its environment, being changed in a similar way upon dilution with either iPP or aPP.

The LJ energy in the 50/50 iPP/aPP melt is in the same range as the LJ energies of the two pure components, which were themselves not very different from one another. All of these energies are within a range of 0.2 kJ/mol. The two 50/50 melts that contain sPP have LJ energies that are less negative than that seen in the pure sPP melt, but more negative than the LJ energy of the second component. The melt LJ energy is larger than the average of the LJ energies of the two components when the system contains sPP.

The energies deduced for sPP in a binary melt with iPP depend on the composition of that blend. Table 3 compares the energies of equilibrated iPP/sPP melts in which the numbers of independent parent chains of the two stereochemical compositions are 9/9 or 17/1, all chains having the same degree of polymerization. The 17/1 mixture has a total energy, as well as LJ and RIS components, that are indistinguishable from the corresponding terms for the one-component melt of the dominant species, iPP (Table 1). However, the RIS energy of sPP is different from that seen in its one-component melt (Table 1) or in the 50/50 blend with iPP (Table 2). The RIS energy of the bead of sPP increases continuously as the sPP is diluted with

iPP, rising from 3.87 ± 0.07 kJ/mol (pure sPP) to 4.61 ± 0.17 kJ/mol for the 50/50 blend to 5.71 ± 0.15 kJ/mol for the 17/1 blend. The implication is that sPP prefers a different distribution of conformations in its own melt and when completely diluted with iPP. On the other hand, the RIS energies suggest that iPP has a similar distribution of conformations in its own melt and in its blends with sPP.

The change in energy upon mixing of the 50/50 mixtures can be calculated from the data in Tables 1 and 2. The result for the iPP/aPP blend, Table 4, is not distinguishable from zero. This result from the simulation is consistent with the miscibility for this system that is observed in experiment, and is also consistent with the absence of strong evidence for phase separation in Figure 6. For the other two melts, there is a positive energy change on mixing that exceeds the standard deviation. This change might be larger for the iPP/sPP melt than for the aPP/sPP melt, but the difference does not exceed the sum of the standard deviations. This result is qualitatively consistent with the reported immiscibility of these two systems. It is also suggestive that the iPP/sPP system is more immiscible than the aPP/sPP system, as seen in the experiments of Mülhaupt and coworkers. However, the sizes of the positive energy changes on mixing of the iPP/sPP or iPP/aPP in the simulation is larger than expected from the experiment. This quantitative disagreement was apparent already in the snapshots of the equilibrated melts (Figures 7 and 8), where significant immiscibility was easily detectable at molecular weights much smaller than those required for the experimental detection of immiscibility at the same temperature. The positive energy change on mixing of the two melts containing sPP has important contributions from both the RIS and LJ components.

Mobility. Significantly different numbers of Monte Carlo steps (MCS) are required for equilibration of the one-component iPP and sPP melts. The mean square displacements of individual beads in eight-chain one-component melts of iPP over a window of 2.5×10^4 MCS (Figure 14) or sPP over a longer window of 8×10^5 MCS (Figure 15) show significantly different mobilities. These two different time windows were chosen because they both provide a mean

square displacement of 40-60 Å^2 per bead when averaged over all beads indexed 10–40, i. e., when ignoring the beads near either end of the chains Although these averaged mobilities are similar, the two figures show that individual beads in individual chains can depart strongly from the average, and the departure is especially interesting in sPP. In the iPP melt, every bead in every chain has a mean square displacement of at least 30 Å^2 during this short time interval, but in the sPP melt, a few beads have not moved at all during the longer time period. Slower correlation times for conformation transitions for sPP than for iPP were reported in a recent MD simulation of their one-component melts,[42] although the difference was not as large as the differences in mobilities in the MC simulation.

The sluggishness of the sPP chains is also observed in the present MC simulation of the 50/50 iPP/sPP melt, as shown in Figure 16, where several beads have negligible movement during the time interval depicted. However, when the sPP is more strongly diluted by iPP, as in the 17/1 iPP/sPP melt, all of the beads of the single sPP chain have a mean square displacement of more than 30 Å^2 during a rather short window of 5×10^4 MCS, as shown in Figure 17. This result demonstrates that the sluggishness of the sPP chains in the simulation of its melt and 50/50 blend is not to be attributed to an inherent intramolecular property of the single chain, but arises instead from the interaction of one sPP chain with another sPP chain in its immediate environment.

Mechanism. The foregoing paragraphs identify three peculiar characteristics of the sPP melts: The pair correlation functions (Figure 13) reveal more structure in the sPP melt than is seen in either the aPP or iPP melt. The decomposition of the energies shows that the RIS energy of sPP depends strongly on the composition of the system in which it occurs (Tables 1–3), but no equivalent composition dependence is observed with aPP or sPP. Finally, analysis of the mobilities of the individual beads in an sPP chains shows increased sluggishness when its environment changes from iPP to sPP (Figures 15–17). These peculiarities suggest a "structure" of the sPP melt which may reduce its tendency to mix with either aPP or iPP.

Some insight into the "structure" can be glean by noticing that the slowly moving beads in individual sPP chains (Figures 16 and 17) are not randomly distributed, but instead tend to occur in short sequences. Inspection of these short sequences in the relevant snapshots shows that the immobile beads form linear segments on the high-coordination lattice, i. e., in the fully atomistic representation, they are short sequences in which all of the C-C bond in the backbone are in *trans* states. The RIS model shows that these sequences are of higher probability in sPP than in either aPP or iPP. Further inspection of the snapshots reveals that the individual immobile segments from different chains are not randomly distributed over the simulation cell, but instead tend to occur in small clusters, each cluster being composed of short segments from different chains. The immobile linear segments in these clusters tend to be colinear, with a preferred lateral spacing of three lattice units. This spacing is also the location of the minimum energy in the discretized version of the LJ potential that was derived from propane.

Presumably these transitory immobile regions initiate from the spontaneous formation of sequences of *trans* placement in sPP, which is a natural consequence of the RIS model for this polymer. No special stabilization of these all-*trans* sequences is possible if the environment of sPP is composed exclusively of iPP chains (Figure 17). The iPP chains prefer *tg* sequences, and rarely form sequences of *trans* placements that can interact with the all-*trans* sequences in an sPP chain. However, if the environment of a sPP chain is composed of other sPP chains, such chains may also spontaneously produce sequences of *trans* placements. If such sequences from two different chains happen to arise in a situation where they are colinear, and separated by a distance that corresponds to the minimum in the LJ potential, their attractive intermolecular interaction causes them to be longer lived than would be the case if they were formed in an environment dominated by iPP. Therefore the sPP chains resist being forced into an environment that is rich in either iPP or aPP. In contrast, iPP and aPP do not discriminate between one another, because neither has a strong tendency to spontaneously form sequences of *trans* placements. Of course, this tendency for runs of *trans* placements might persist to a slight extent in aPP, because Bernoullian statistics do allow the occasional stringing together of several

racemo diads in such chains. These naturally occurring strings of *racemo* diads in aPP may account for the slightly greater mixing of sPP with aPP, as compared to sPP with iPP.

Comparison of the Two Approaches

Both simulations deduce a positive energy of mixing for iPP/sPP in the melt. This energy is larger in the RIS/MC simulation than in the MC/PRISM calculation. The latter result gives a molecular weight dependence for the demixing that is closer to the behavior reported by Mülhaupt and coworkers for this system. Refinement in one or more of the parameters in the RIS/MC simulation might improve its quantitative agreement with experiment.

The RIS/MC simulation finds an energy of mixing that is indistinguishable from zero for iPP/aPP, a result compatible with experiments in the literature for this system. The treatment of aPP is easier in the RIS/MC simulation than in the MC/PRISM calculation because the former method employs several independent parent chains, each of which can have its own stereochemical sequence in the representation of aPP. Since the MC/PRISM calculation takes its detailed local conformational information from a single chain, it would have to treat the aPP system as a chain with a mixture of *meso* and *racemo* diads, that is arranged in a specific sequence. The mixing of iPP/aPP has not been studied with MC/PRISM.

The MC/PRISM calculation operates in continuous space, but the RIS/MC simulation uses the discrete space of a high coordination lattice, with $10i^2 + 2$ sites in shell i. Reverse-mapping of equilibrated replicas from the RIS/MC simulation causes the chains to fall into a nearby local minimum in continuous configuration space. However, this minimum is located very close to the coordinates of the chains on the lattice because reverse-mapping does not produce large-scale rearrangement of the chains.

Both calculations use coarse-grained monomer units, but they differ in the degree of coarse-graining. MC/PRISM represents the propylene unit with three distinct sites, one for each of the distinguishable carbon atoms, whereas the RIS/MC calculation represents the propylene

unit with a single site, located at the coordinates of the carbon atom that bears the methyl side chain. Reverse-mapping of individual replicas in the RIS/MC simulation restores all of the carbon and hydrogen atoms, but only after prior equilibration using the coarse-grained representation of the chains.

The potential energy function for the intermolecular interactions is based on an LJ potential but the implementation is different in the two approaches. The RIS/MC simulation uses a single Lennard-Jones potential for all of the coarse-grained propylene units, independent of the stereochemical composition of the chain. The MC/PRISM calculation uses a more detailed description of the monomer unit, which requires several Lennard-Jones functions with slightly different values of ε and σ. The MC/PRISM approach must assume the validity of the Berthelot mixing rules, but the RIS/MC approach makes no appeal to these rules because the entire simulation uses only one ε and one σ. The Lennard-Jones potential energy is continuous and spherically symmetric in the MC/PRISM calculation, but it is discretized and directional in its use on the high coordination lattice in the RIS/MC simulation.

The input for the local conformational properties comes from a MC simulation of an oligomer in the MC/PRISM calculation and from a rotational isomeric state model in the RIS/MC simulation.

The MC/PRISM calculation uses shorter chains (degree of polymerization of 12) than does the RIS/MC simulation (degree of polymerization of 50). The ends account for 17% and 4% of the units, respectively, in the two simulations.

In both methods, individual calculations are performed at constant density. This constant density depends on the composition of the system in the MC/PRISM calculation (with a different of 0.3% in the densities of iPP and sPP), but not in the RIS/MC calculation. The set of RIS/MC calculations is performed in a manner that assumes no change in volume on mixing, whereas a change in volume upon mixing is incorporated in the MC/PRISM calculation. In the results reported here, the densities are about 1% lower in the RIS/MC simulation than in the MC/PRISM calculation, reflecting the fact that the former was performed at 473K, but the latter was at 453K.

The use of several discrete and independent parent chains in the RIS/MC simulation permits detection of very small, short-lived intermolecular aggregates in the sPP melt. The use of shorter chains, the avoidance of discrete representation of neighboring chains, and the absence of "time" expressed in MCS might make detection of such small, short-lived aggregates more difficult in the MC/PRISM calculation.

Acknowledgments

This work was supported by NSF DMR 9523278 and .....(Curro). WLM thanks JGC for his hospitality while he was on sabbatical leave at Sandia National Laboratory.

References and Notes

(1) Lohse, D J. *Polym. Eng. Sci.* **1986**, *26*, 1500.

(2) Thomann, R.; Kressler, J.; Setz, S.; Wang, C.; Mülhaupt, R. *Polymer* **1996**, *37*, 2627.

(3) Thomann, R.; Kressler, J.; Rudolf, B.; Mülhaupt, R. *Polymer* **1996**, *37*, 2635.

(4) Maier, R. D.; Thomann, R.; Kressler, J,; Mülhaupt, R.; Rudolf, B. *J. Polym. Sci. B* **1997**, *35*,1135.

(5) Schweizer, K. S.; Curro, J. G. *Adv. Polym. Sci.* **1994**, *116*, 321.

(6) Schweizer, K. S.; Curro, J. G. *Adv. Chem. Phys.* **1997**, *98*, 1.

(7) Baschnagel, J.; Binder, K.; Doruker, P.; Gusev, A. A.; Hahn, O.; Kremer, K.; Mattice, W. L.; Müller-Plathe, F.; Murat, M.; Paul, W.; Santos, S.; Suter, U. W.; Tries, V. *Adv. Polym. Sci.* **2000**, *152*, 41.

(8) Doruker, P.; Mattice, W. L. *Macromol. Theory Simul.* **1999**, *8*, 463.

(9) Schweizer, K. S.; Curro, J. G. *Phys. Rev. Lett.* **1987**, *58*, 246.

(10) Curro, J. G.; Schweizer, K. S. *Macromolecules* **1987**, *20*, 1928.

(11) Curro, J. G.; Schweizer, K. S. *J. Chem. Phys.* **1987**, *87*, 1842.

(12) Chandler, D.; Andersen, H. C. *J. Chem. Phys.* **1972**, *57*, 1930.

(13) Chandler, D. in Studies in Statistical Mechanics VIII, Montroll, E. W.; Lebowitz, J. L., Eds., North-Holland: Amsterdam, 1982.

(14) Martin, M. G.; Siepmann, J. I. *J. Phys. Chem. B* **1999**, *103*, 4508.

(15) Pütz, M.; Curro, J. G.; Grest, G. S. *J. Chem. Phys.* **2000**, *000*, 0000.

(16) Hansen, J. P.; Mcdonald, I. R. Theory of Simple Liquids, 2nd ed., Academic: New York. 1986.

(17) Tillman, P. A.; Rottach, D. R.; McCoy, J. D.; Plimpton, S. J.; Curro, J. G. *J. Chem. Phys.* **1997**, *107*, 4024.

(18) Tillman, P. A.; Rottach, D. R.; McCoy, J. D.; Plimpton, S. J.; Curro, J.G. *J. Chem. Phys.* **1998**, *109*, 806.

(19) Weeks, J. D.; Chandler, D.; Andersen, H. C. *J. Chem. Phys.* **1971**, *54*, 5237.

(20) Weinhold, J. D.; Curro, J. G.; Habenschuss, A.; Londono, J. D. *Macromolecules* **1999**, *32*, 7276.

(21) Flory, P. J. *J. Chem. Phys.* **1949**, *17*, 203.

(22) Curro, J. G.; Weinhold, J. D.; Rajasekaran, J. J.; Habenschuss, A.; Londono, J. D.; Honeycutt, J. D. *Macromolecules* **1997**, *30*, 6264.

(23) Curro, J. G.; Webb, E. B.; Grest, G. S.; Weinhold, J. D.; Pütz, M.; McCoy, J. D. *J. Chem. Phys.* **1999**, *111*, 9073.

(24) Stevenson, C. S.; McCoy, J. D.; Plimpton, S. J.; Curro, J. G. *J. Chem. Phys.* **1995**, *103*, 1200.

(25) Stevenson, C. S.; Curro, J. G.; McCoy, J. D.; Plimpton, S. J. *J. Chem. Phys.* **1995**, *103*, 1208.

(26) Gromov, D. G.; de Pablo, J. J. *J. Chem. Phys.* **1998**, *109*, 10042.

(27) Kirkwood, J. G.; Buff, F. P. *J. Chem. Phys.* **1951**, *19*, 774.

(28) Flory, P. J. Principles of Polymer Chemistry, Cornell Univ. Press, Ithaca, New York, 1953.

(29) Flory, P.J. Statistical Mechanics of Chain Molecules, Wiley, New York, 1969.

(30) Mattice, W. L.; Suter, U. W. Conformational Properties of Large Molecules. The Rotational Isomeric State Model in Macromolecular Systems, Wiley, New York, 1994.

(31) Rapold, R. F.; Mattice, W. L. *Macromolecules* **1996**, *29*, 2457.

(32) Cho, J.; Mattice, W. L. *Macromolecules* **1997**, *30*, 637.

(33) Haliloglu, T.; Cho, J.; Mattice, W. L. *Macromol. Theory Simul.* **1999**, *7*, 613.

(34) Haliloglu, T.; Mattice, W. L. *J. Chem. Phys.* **1998**, *108*, 6989.

(35) Reid, R. C.; Prausnitz, J. M.; Poling, B. E. The Properties of Gases and Liquids, 4th ed., p 773.

(36) Doruker, P.; Mattice, W. L. *Macromolecules* **1997**, 30, 5520.

(37) Haliloglu, T.; Mattice, W. L. *J. Chem. Phys.* **1999**, *111*, 4327.

(38) Clancy, T. C.; Mattice, W. L. *J. Chem. Phys.*, in press.

(39) Suter, U. W.; Pucci, S.; Pino, P. *J. Am. Chem. Soc.* **1975**, *97*, 1018.

(40) Eckstein, A.; Sulm, J.; Friedrich, C.; Maier, R.-D.; Sassmannshausen, J.; Bochmann, M.; Mülhaupt, R. *Macromolecules* **1998**, *31*, 1335.

(41) Orwoll, R. A. in Physical Properties of Polymer Handbook, Mark, J. E., Ed., American Institute of Physics, Woodbury, New York, **1996**, p 81.

(42) Antoniadis, S. J.; Samara, C. T.; Theodorou, D. N. *Macromolecules* **1999**, *32*, 8635.

Figure Legends

Figure 1. Schematic representation of a united atom model of PP. The A type sites refer to CH_2, B type sites to CH, and C type sites to CH_3 groups. The bond lengths, bond angles, and torsional potentials are taken from ref 14. The stereochemistry of either the isotactic or syndiotactic placement of the C sites is preserved.

Figure 2. The average pair correlation functions of iPP and sPP in the 50/50 blend. The solid curves refer to the pure component liquids and the points to the mixture. The dotted line is the average over all the cross correlation functions between iPP and sPP chains in the blend.

Figure 3. The pair correlation functions between the pairs of sites shown in the figure. The solid curves refer to the pure component liquids and the points to the mixture. The dotted curves represent the cross correlations between pairs of sites on chains of different tacticity in the blend. The results for the CH_2/CH_2 and CH/CH pairs have been shifted along the $g(r)$ axis for clarity.

Figure 4. Pair correlations between CH_3 and CH_2 sites. The solid curves refer to the pure component liquids and the points to the mixture. The two dotted curves represent the cross correlations between chains of different tacticity in the blend. Note that the CH_3 sites on iPP have a preference for CH_2 sites on sPP (curve iPP/sPP) and the opposite is true for CH_3 sites on sPP and CH_2 sites on iPP (curve sPP/iPP).

Figure 5. The heat of mixing per monomer divided by k_BT of the iPP/sPP blend for $N = 12$ monomers per chain at $T = 453$K plotted against the volume fraction of iPP monomers ϕ. The points were computed from self-consistent PRISM theory and equation 10. The solid curve

through the points is a guide to the eye. The dotted curve was an estimate based on the solubility parameters of the pure components.

Figure 6. Snapshot of the carbon atoms in a reverse-mapped periodic cell for an equilibrated melt containing equal numbers (nine each) of coarse-grained iPP (lighter spheres) and aPP (darker spheres) chains at 473K and a density of 0.750 g/cm^3.

Figure 7. Snapshot of the carbon atoms in a reverse-mapped periodic cell for an equilibrated melt containing equal numbers of coarse-grained iPP (lighter spheres) and sPP (darker spheres) chains at 473Kand a density of 0.750 g/cm^3.

Figure 8. Snapshot of the carbon atoms in a reverse-mapped periodic cell for an equilibrated melt containing equal numbers of coarse-grained aPP (lighter spheres) and sPP (darker spheres) chains at 473K and a density of 0.750 g/cm^3.

Figure 9. Intermolecular pair correlation functions for carbon atoms in a reverse-mapped 50/50 iPP/aPP blend at 473K and a density of 0.750 g/cm^3. The correlation functions are for all carbon atoms (gray line with circles), carbon atoms in iPP (solid line) or aPP (heavy dashed line), or the cross-correlation of iPP with aPP (light dashed line).

Figure 10. Intermolecular pair correlation functions for carbon atoms in a reverse-mapped 50/50 aPP/sPP blend at 473K and a density of 0.750 g/cm^3. The correlation functions are for all carbon atoms (gray line with circles), carbon atoms in sPP (solid line) or aPP (heavy dashed line), or the cross-correlation of iPP with aPP (light dashed line).

Figure 11. Intermolecular pair correlation functions for carbon atoms in a reverse-mapped 50/50 iPP/sPP blend at 473K and a density of 0.750 g/cm^3. The correlation functions are for all carbon atoms (gray line with circles), carbon atoms in iPP (solid line) or sPP (heavy dashed line), or the cross-correlation of iPP with sPP (light dashed line).

Figure 12. Intermolecular pair correlation functions, using all carbon atoms from reverse-mapped replicas, for 50/50 blends of iPP/aPP (heavy dashed line), aPP/sPP (light dashed line), and iPP/sPP (solid line with spheres) at 473K and a density fo 0.750 g/cm^3. These three curves are the "total" curves from the previous three figures.

Figure 13. Intermolecular pair correlation functions, using all carbon atoms from reverse-mapped replicas, for one-component melts aPP (heavy dashed line), iPP (light dashed line), and sPP (solid line with spheres) at 473K and a density of 0.750 g/cm^3.

Figure 14. Mean square displacement during 2.5 $\times 10^4$ MCS for the 50 individual beads in eight independent parent chains of iPP in its one-component melt at 473K and a density of 0.750 g/cm^3.

Figure 15. Mean square displacement during 8 $\times 10^5$ MCS for the 50 individual beads in eight independent parent chains of sPP in its one-component melt at 473K and a density of 0.750 g/cm^3.

Figure 16. Mean square displacement during 4 $\times 10^5$ MCS for the 50 individual beads in nine independent parent chains of sPP in a 50/50 iPP/sPP melt at 473K and a density of 0.750 g/cm^3.

Figure 17. Mean square displacement during 5×10^4 MCS for the 50 individual beads in the single parent chain of sPP in the 17/1 iPP/sPP blend at 473K and a density of 0.750 g/cm^3.

Table 1. Energy per monomer (kJ/mol, ± standard deviation) for coarse-grained one-component PP melts at 473K and a density of 0.750 g/cm^3

Stereochemistry	Total energy	RIS energy	LJ energy
iPP	4.74 ± 0.07	6.99 ± 0.03	-2.25 ± 0.05
aPP	3.88 ± 0.15	6.36 ± 0.07	-2.48 ± 0.09
sPP [a]	-1.16 ± 0.10	3.87 ± 0.07	-5.02 ± 0.07
sPP [b]	-0.96 ± 0.30	3.97 ± 0.14	-4.93 ± 0.17

[a] From discarding the first seven million MC steps, and averaging over the final two million MC steps.

[b] From discarding the first five million MC steps, and averaging over the final four million MC steps.

Table 2. Average energy per bead (kJ/mol ± standard deviation) in the coarse-grained 50/50 two-component PP melts at 473K and 0.750 g/cm^3.

Energy	iPP/aPP	aPP/sPP	iPP/sPP
Total energy	4.44 ± 0.05	1.98 ± 0.33	2.75 ± 0.23
RIS (iPP)	7.07 ± 0.03	- - -	7.09 ± 0.3
RIS (aPP)	6.37 ± 0.03	6.18 ± 0.05	- - -
RIS (sPP)	- - -	4.66 ± 0.19	4.61 ± 0.17
RIS (total)	6.72 ± 0.03	5.42 ± 0.10	5.85 ± 0.09
LJ	-2.28 ± 0.03	-3.45 ± 0.23	-3.10 ± 0.14

Table 3. Average energy per monomer (kJ/mol ± standard deviation) for two compositions of a coarse-grained iPP/sPP melt at 473K and 0.750 g/cm^3.

Energy	9/9 iPP/sPP [a]	17/1 iPP/sPP
Total energy	2.75 ± 0.23	4.72 ± 0.05
RIS (iPP)	7.09 ± 0.03	7.02 ± 0.03
RIS (sPP)	4.61 ± 0.17	5.71 ± 0.15
RIS (total)	5.85 ± 0.09	6.95 ± 0.03
LJ	-3.10 ± 0.14	-2.23 ± 0.03

[a] From Table 2

Table 4. Average change in energy per bead (kJ/mol ± standard deviation) upon mixing of the coarse-grained two-component PP melts at 473K and 0.750 g/cm^3.

Energy	iPP/aPP	aPP/sPP	iPP/sPP
ΔE, total	0.13 ± 0.17	0.61 ± 0.36	0.94 ± 0.34
ΔE, RIS	0.05 ± 0.08	0.30 ± 0.17	0.42 ± 0.14
ΔE, LJ	0.08 ± 0.10	0.30 ± 0.29	0.54 ± 0.20

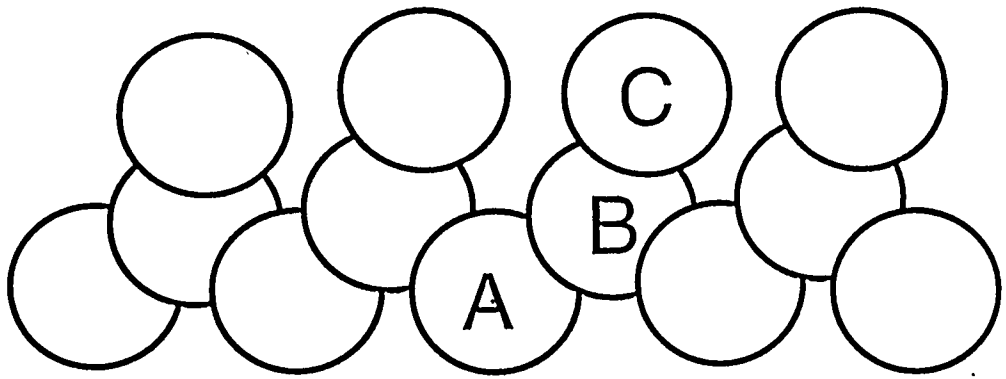
C
B
A

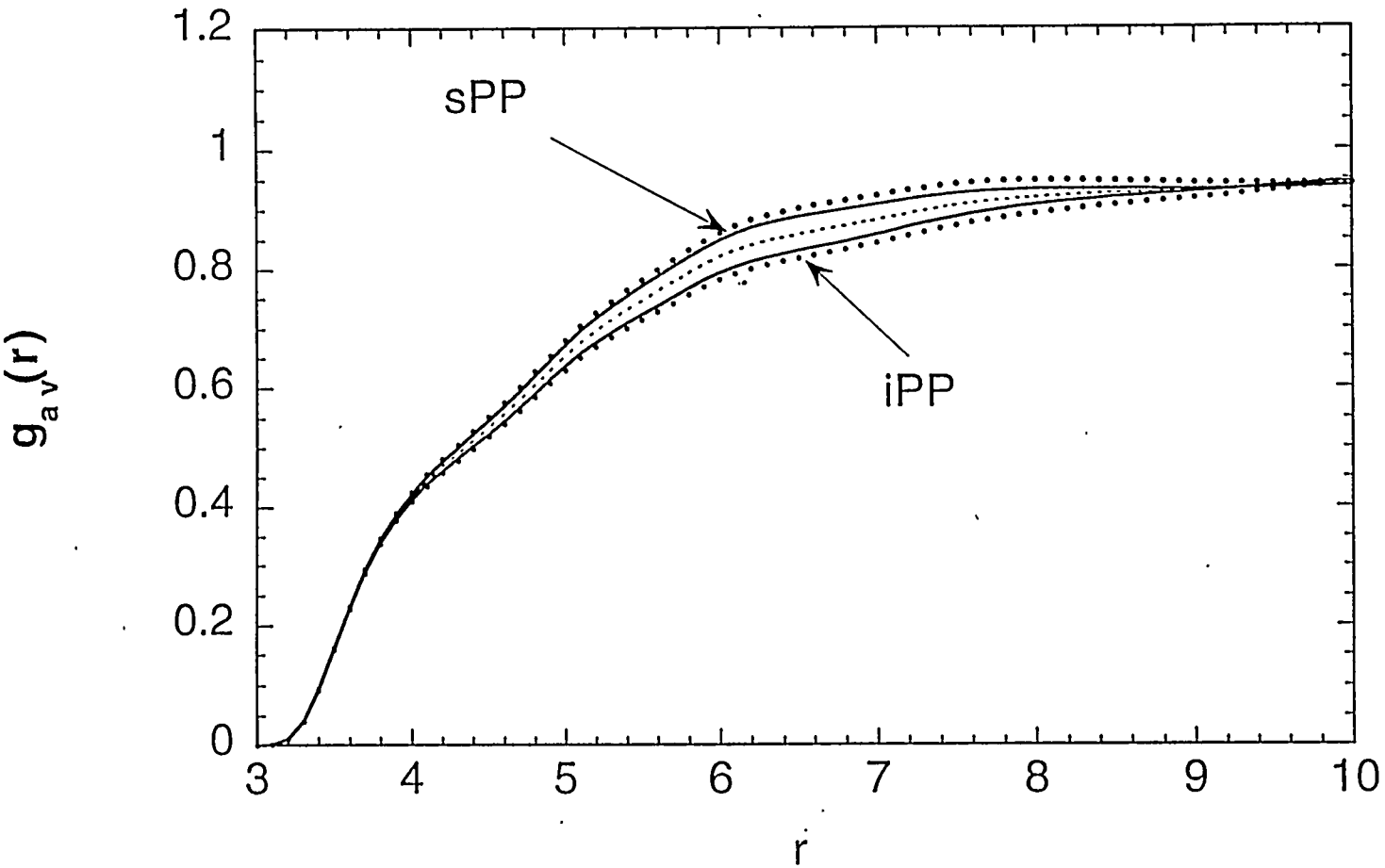
1.2
1
0.8
0.6
0.4
0.2
0
3
4
5
6
7
8
9
10
r
$g_{av}(r)$
sPP
iPP

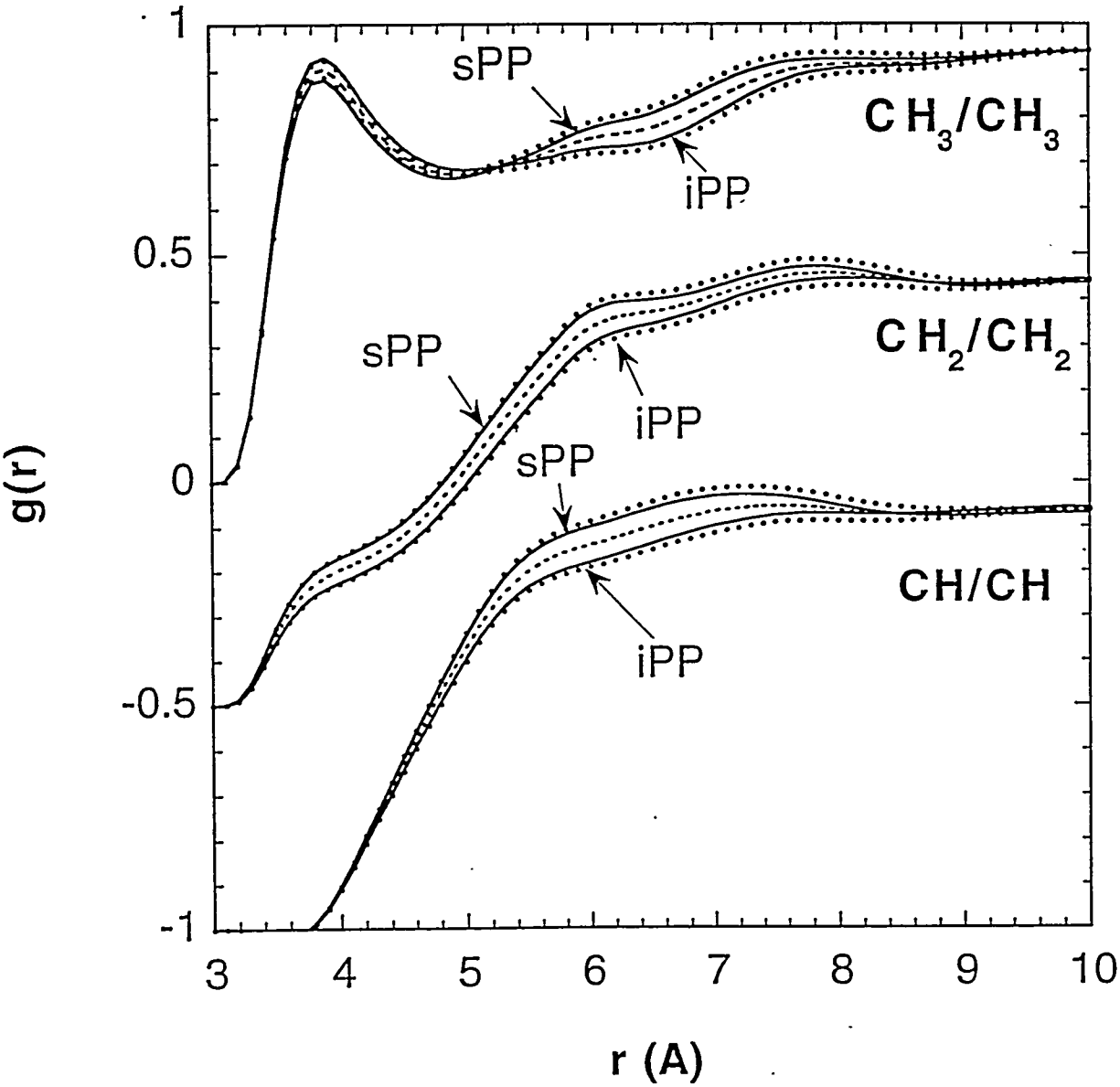
1
0.5
0
-0.5
-1
g(r)
3
4
5
6
7
8
9
10
r (A)
sPP
iPP
CH3/CH3
sPP
iPP
CH2/CH2
sPP
iPP
CH/CH

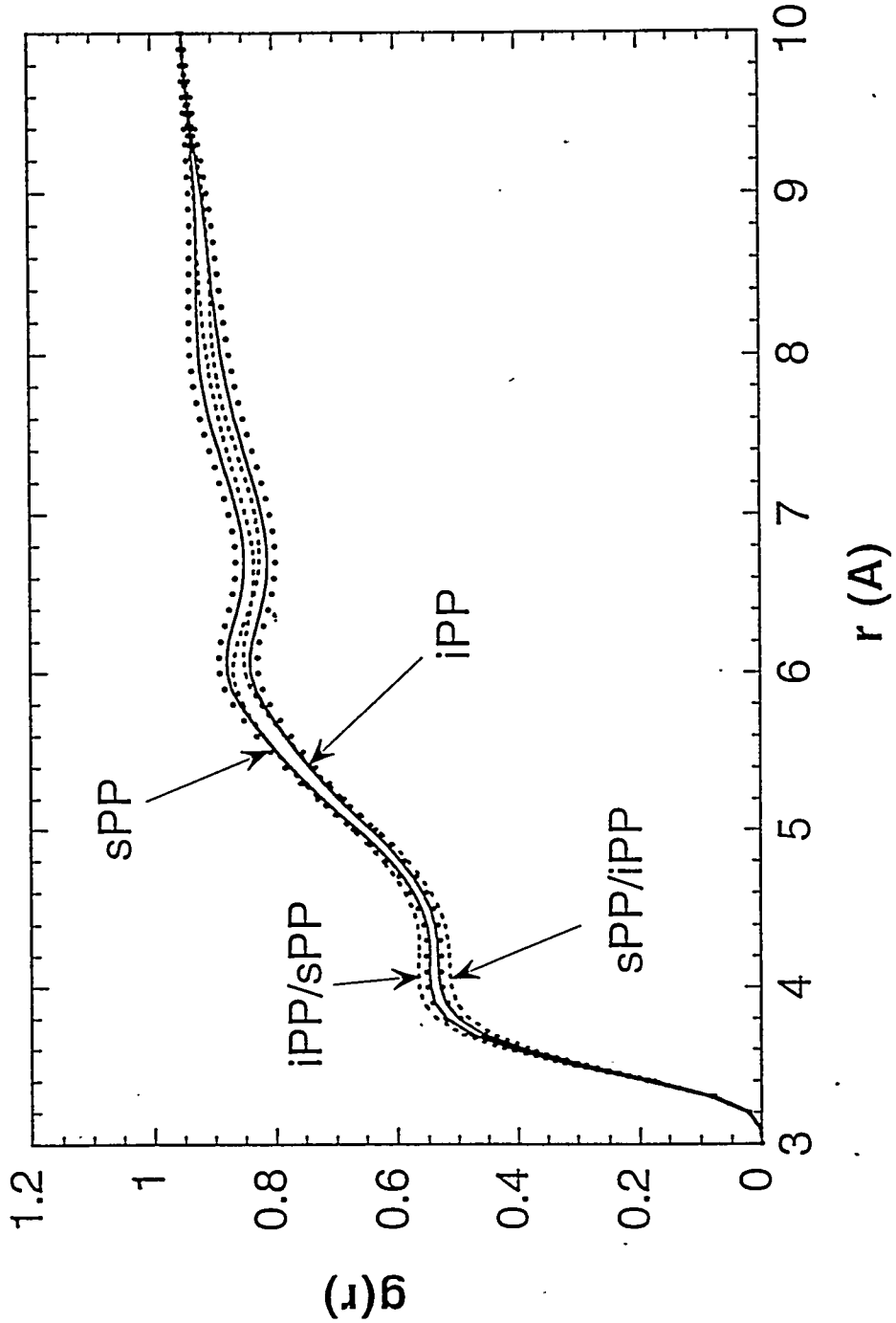
g(r)
r (A)
sPP
iPP
iPP/sPP
sPP/iPP
1.2
1
0.8
0.6
0.4
0.2
0
3
4
5
6
7
8
9
10

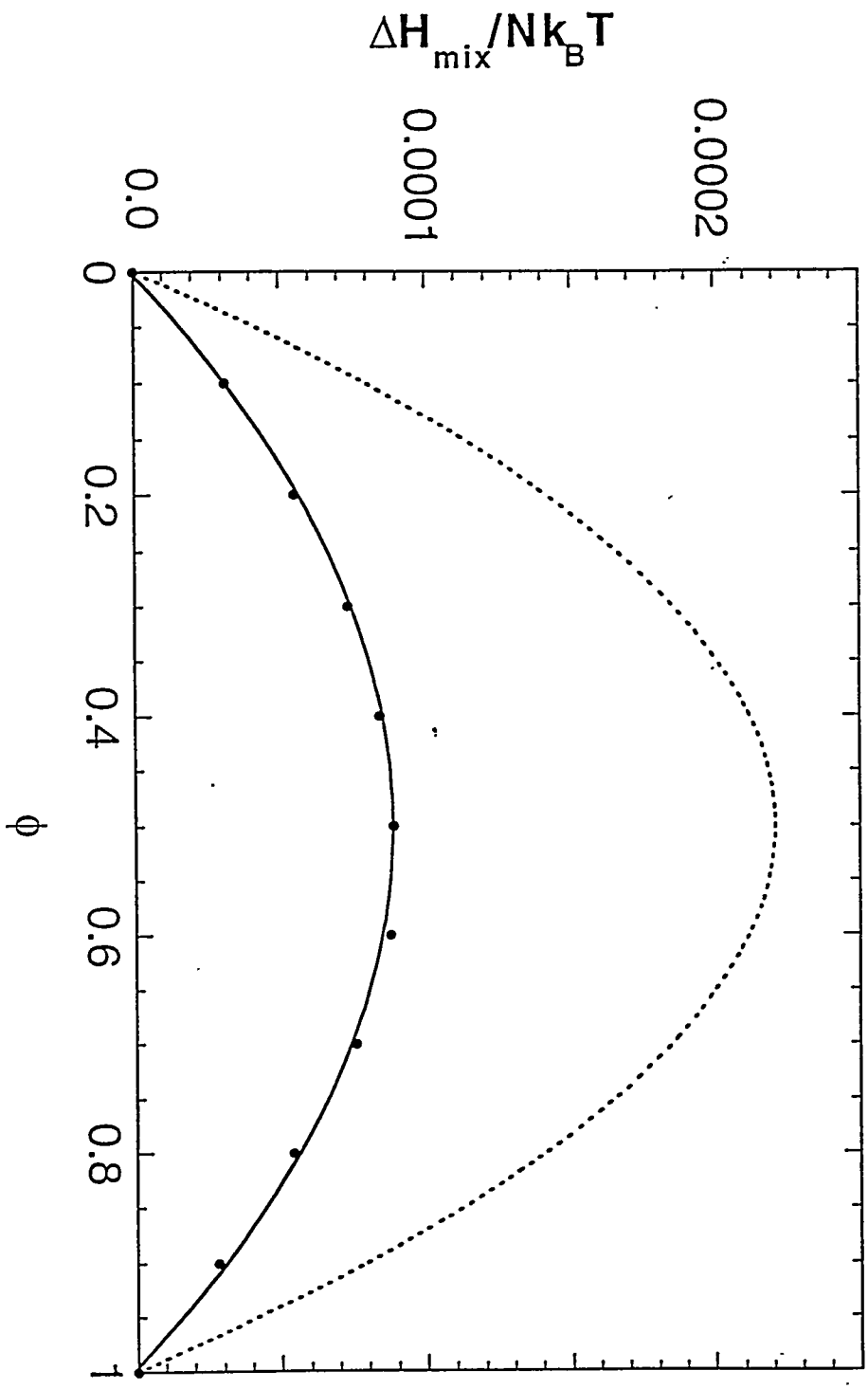

5

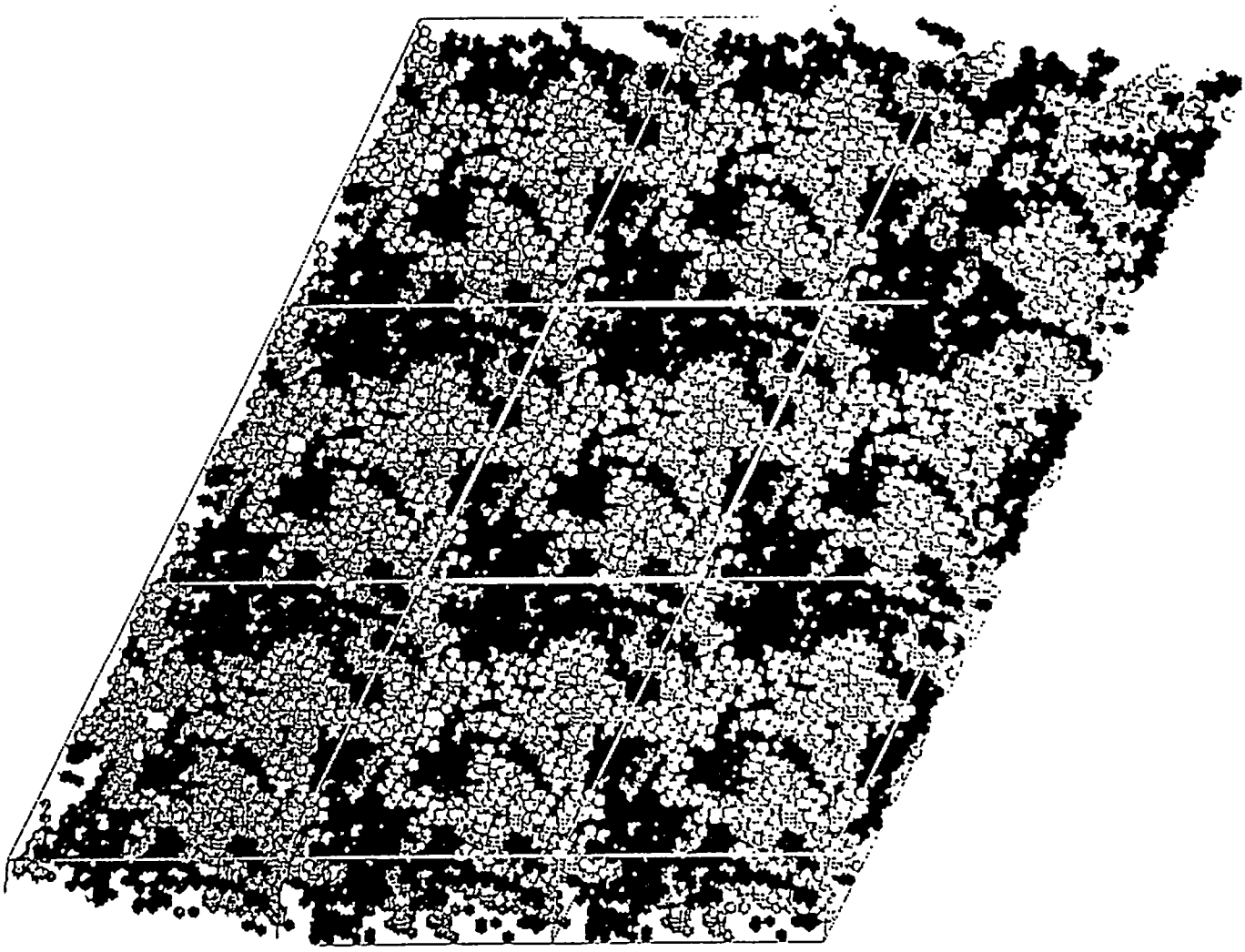

Fig 6

Fig 7

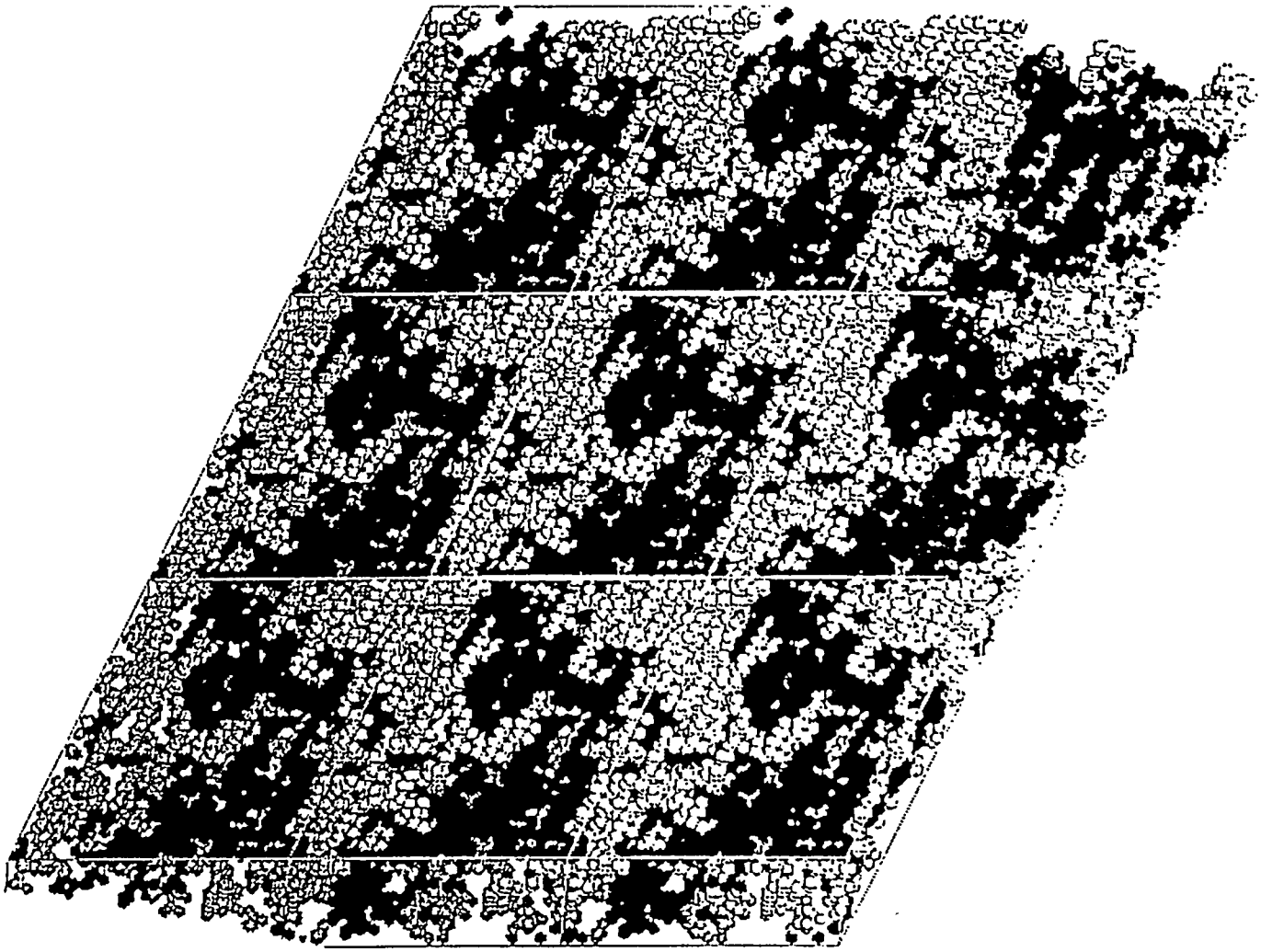

fig 8

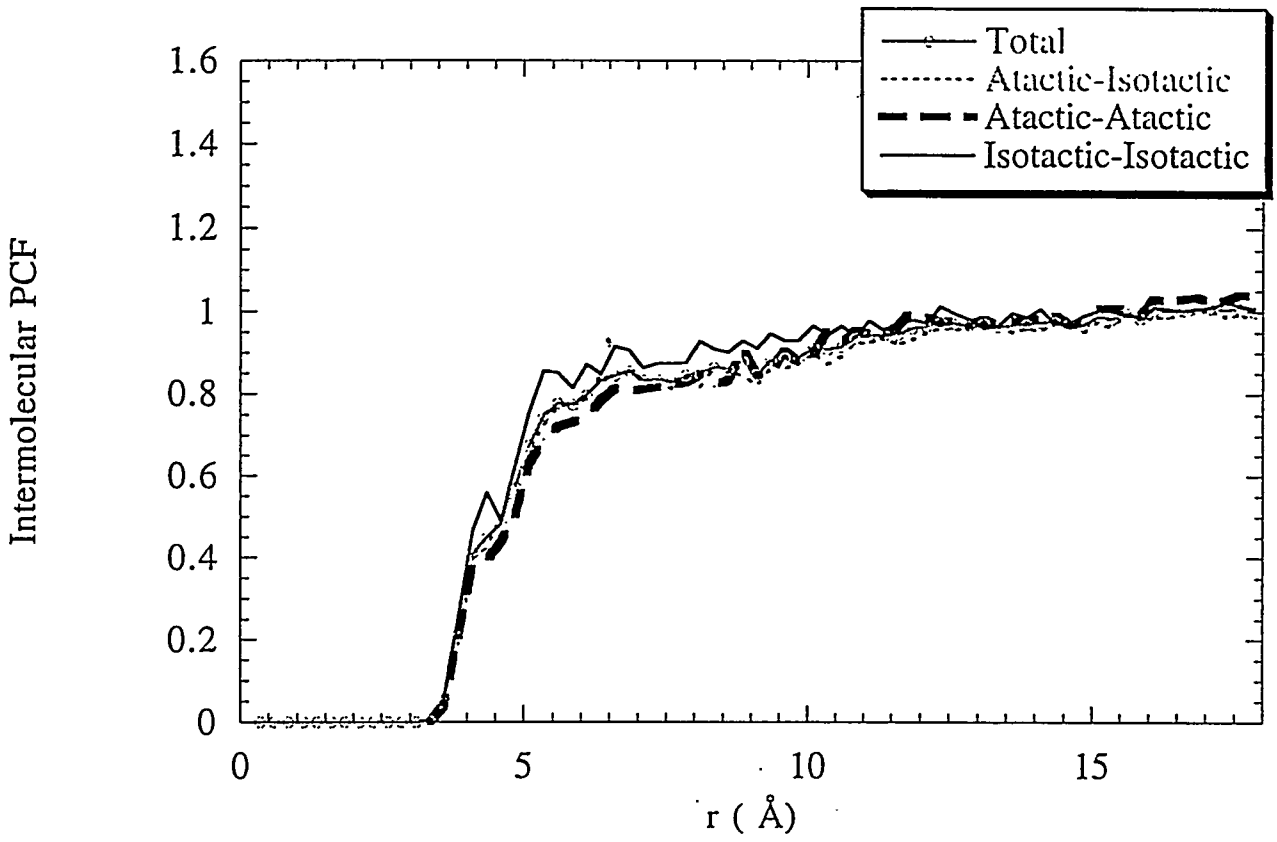
Total
Atactic-Isotactic
Atactic-Atactic
Isotactic-Isotactic
Intermolecular PCF
1.6
1.4
1.2
1
0.8
0.6
0.4
0.2
0
0
5
10
15
r (Å)

fig 9

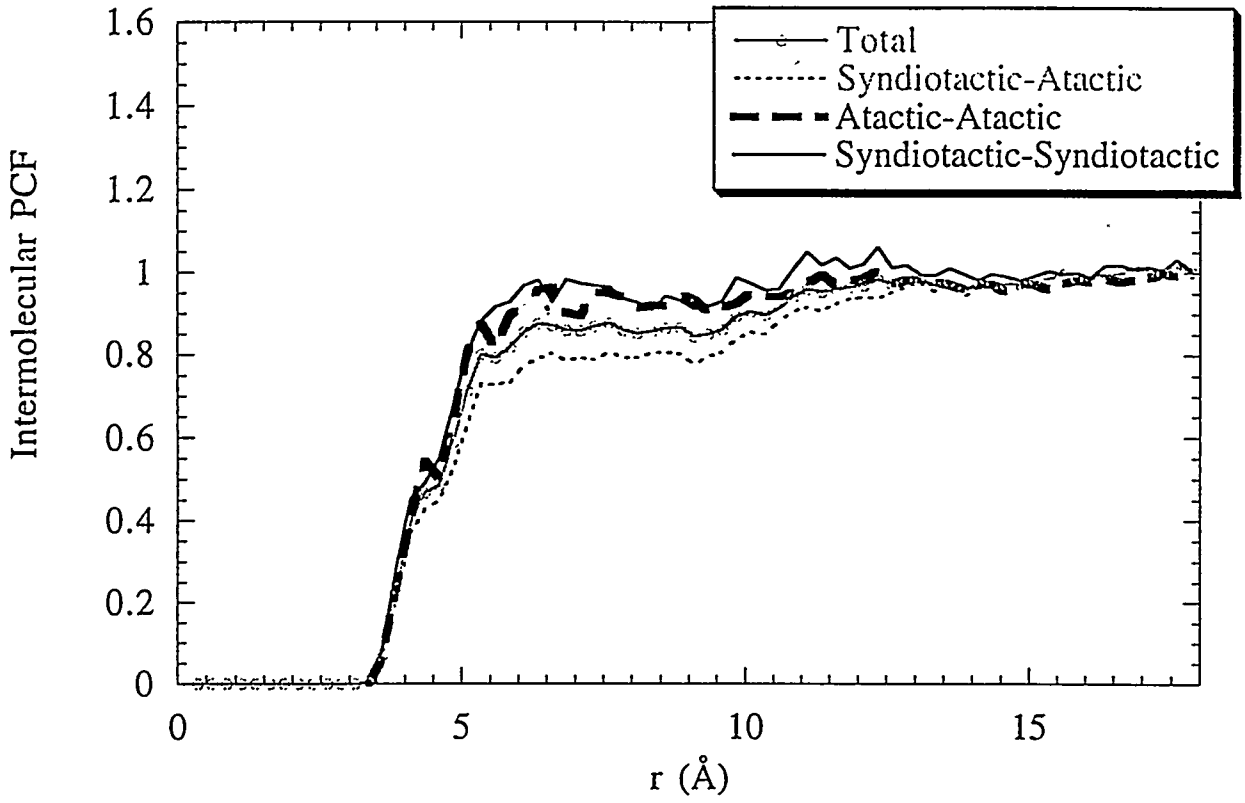
Intermolecular PCF
1.6
1.4
1.2
1
0.8
0.6
0.4
0.2
0
0
5
10
15
r (Å)
Total
Syndiotactic-Atactic
Atactic-Atactic
Syndiotactic-Syndiotactic

fig 10

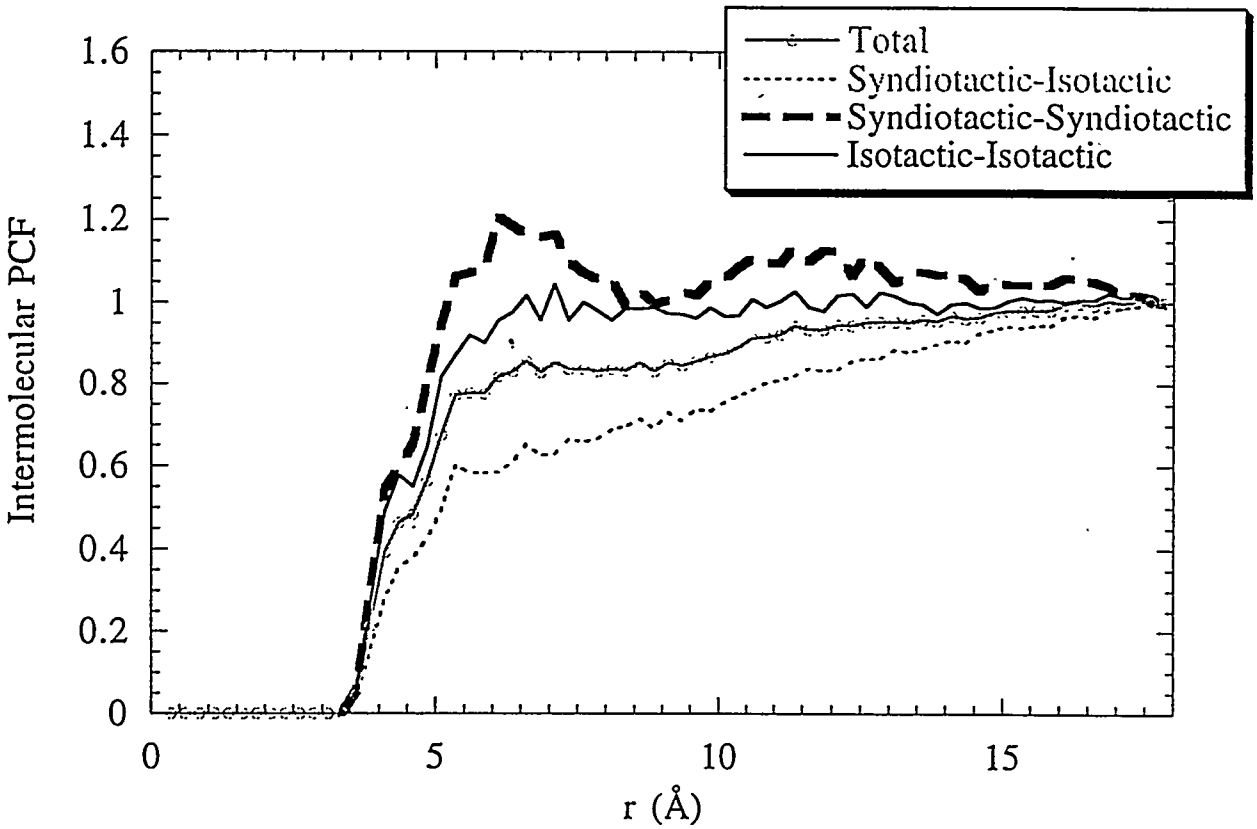
Total
Syndiotactic-Isotactic
Syndiotactic-Syndiotactic
Isotactic-Isotactic
Intermolecular PCF
1.6
1.4
1.2
1
0.8
0.6
0.4
0.2
0
0
5
10
15
r (Å)

fig 11

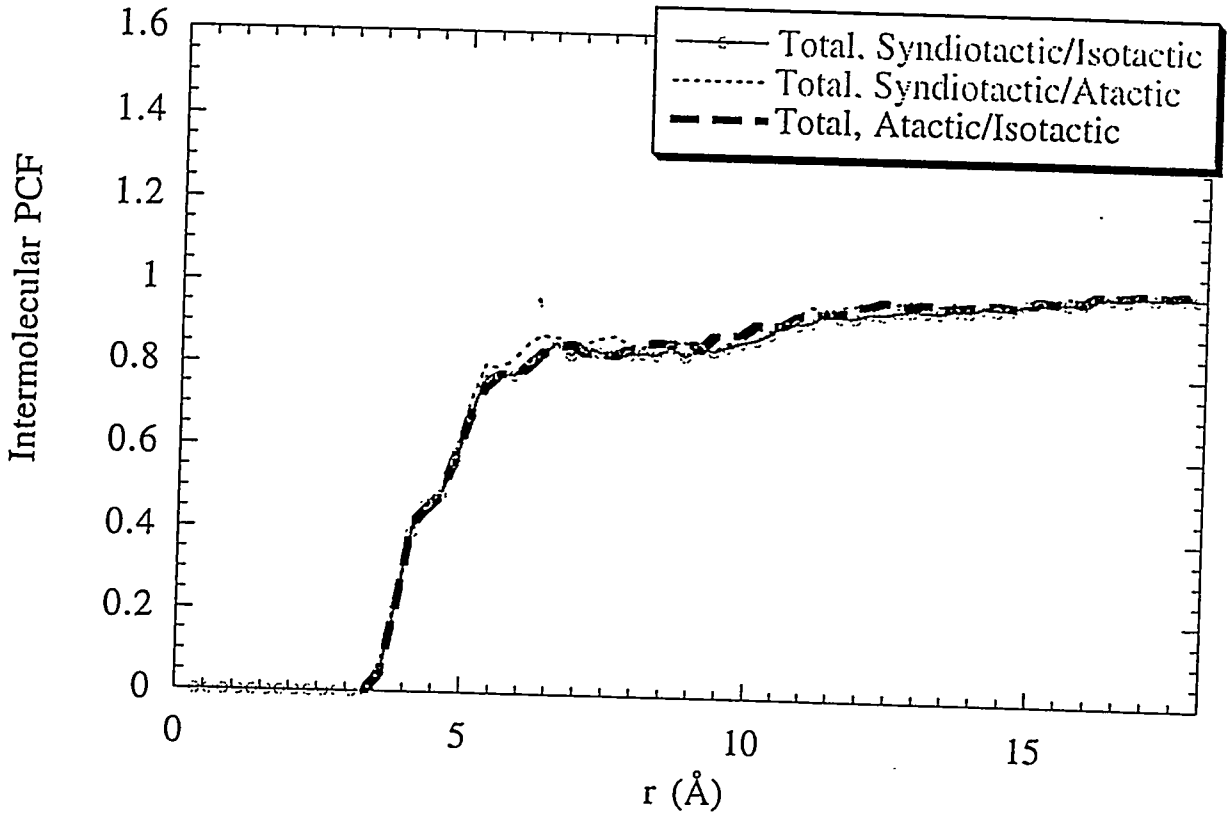
Total. Syndiotactic/Isotactic
Total. Syndiotactic/Atactic
Total, Atactic/Isotactic
Intermolecular PCF
1.6
1.4
1.2
1
0.8
0.6
0.4
0.2
0
0
5
10
15
r (Å)

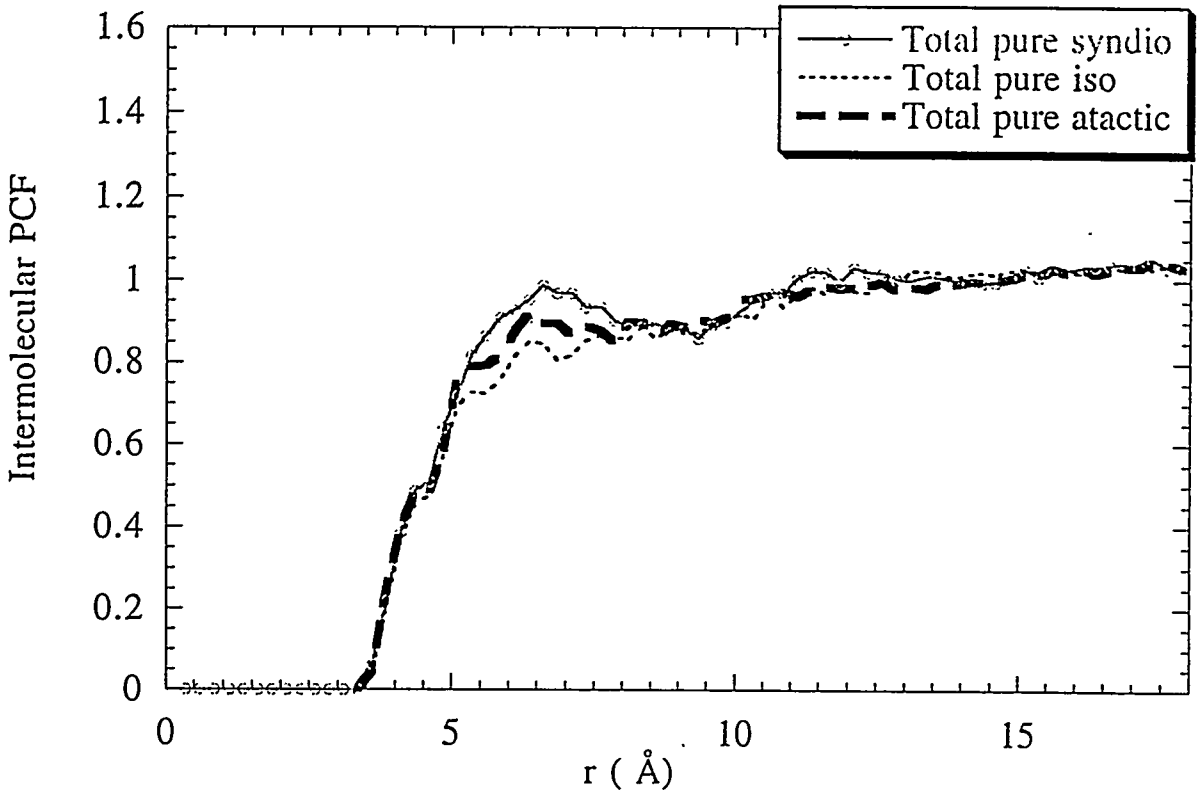
Total pure syndio
Total pure iso
Total pure atactic
Intermolecular PCF
1.6
1.4
1.2
1
0.8
0.6
0.4
0.2
0
0
5
10
15
r (Å)

fig 1

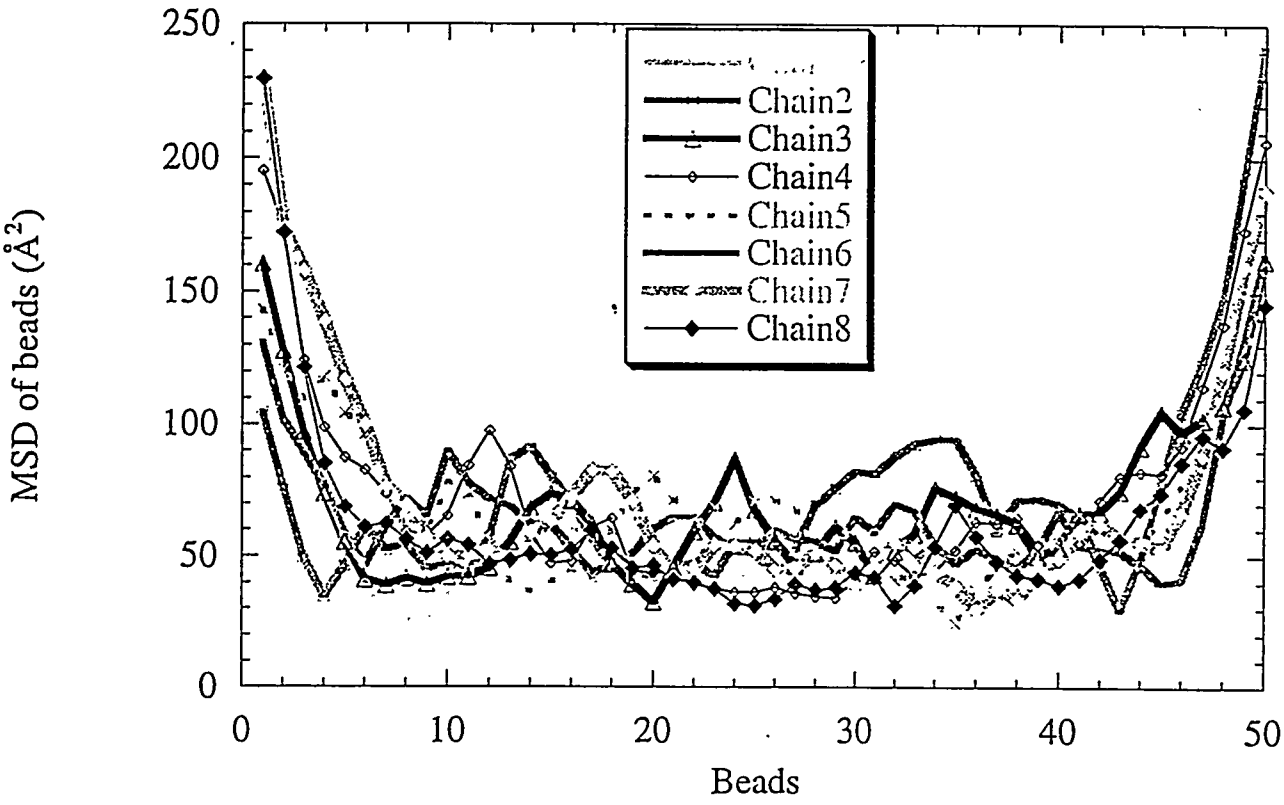
MSD of beads (Å²)
250
200
150
100
50
0
0
10
20
30
40
50
Beads
Chain2
Chain3
Chain4
Chain5
Chain6
Chain7
Chain8

fig 14

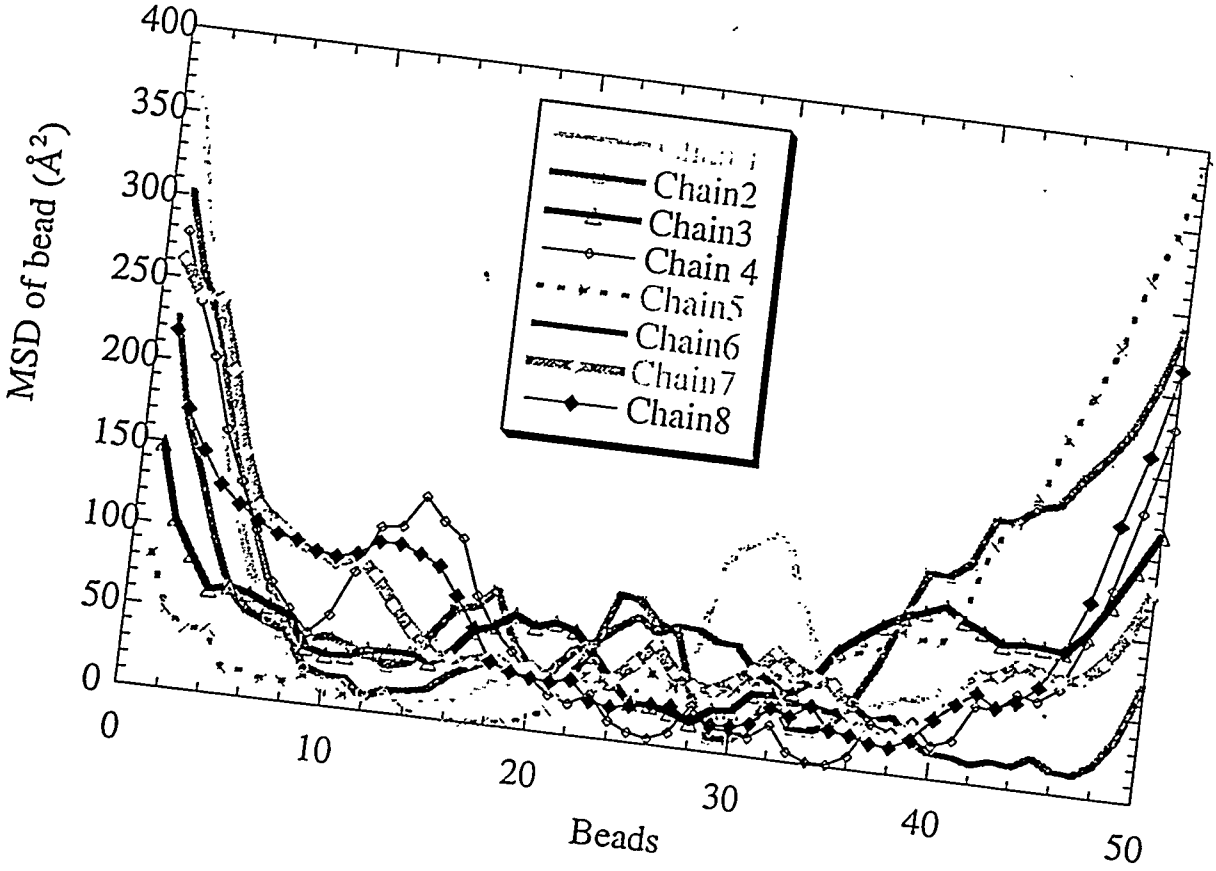
MSD of bead (Å²)
400
350
300
250
200
150
100
50
0
0
10
20
30
40
50
Beads
Chain2
Chain3
Chain 4
Chain5
Chain6
Chain7
Chain8

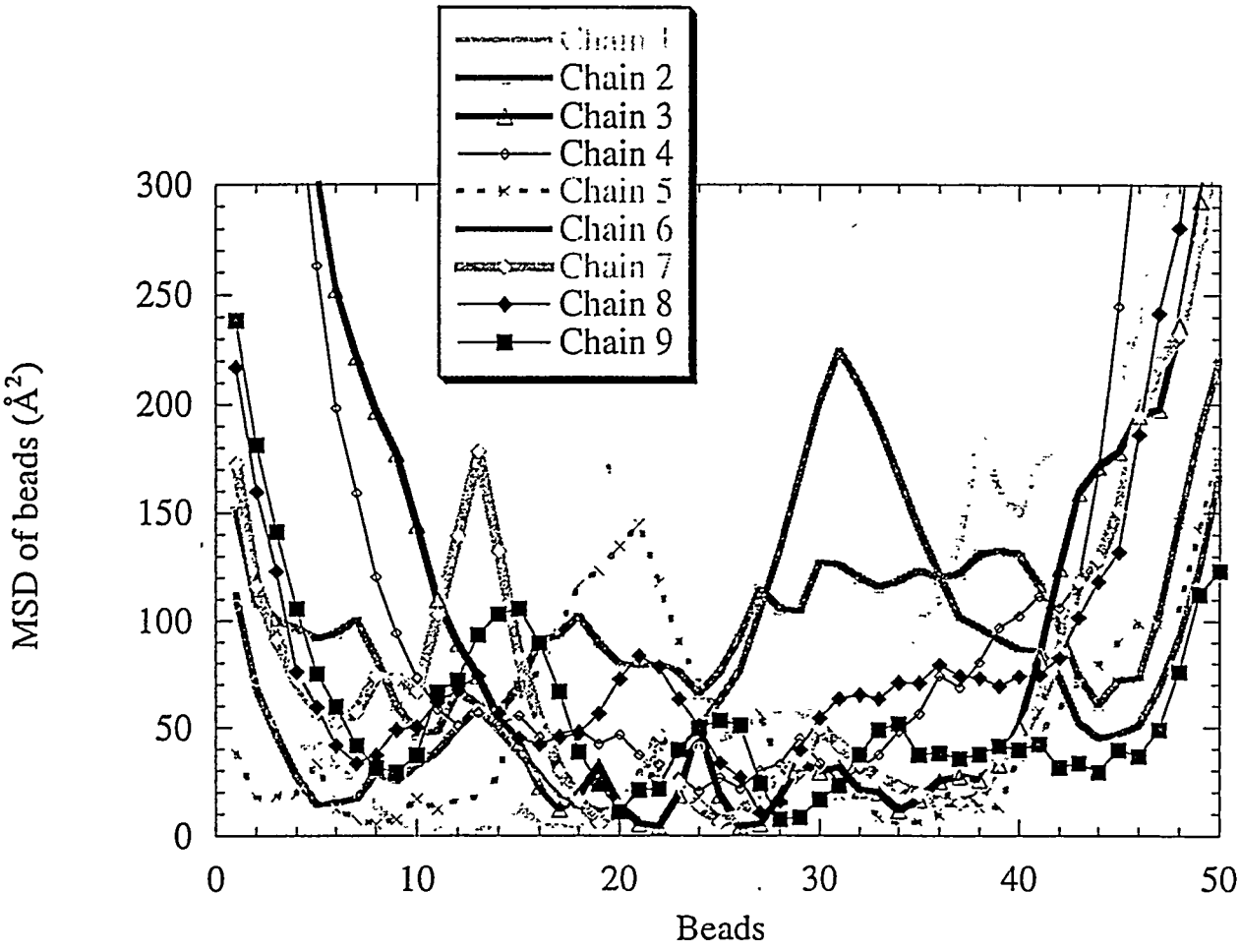
Chain 1
Chain 2
Chain 3
Chain 4
Chain 5
Chain 6
Chain 7
Chain 8
Chain 9
MSD of beads (Å²)
300
250
200
150
100
50
0
0
10
20
30
40
50
Beads

fig 16

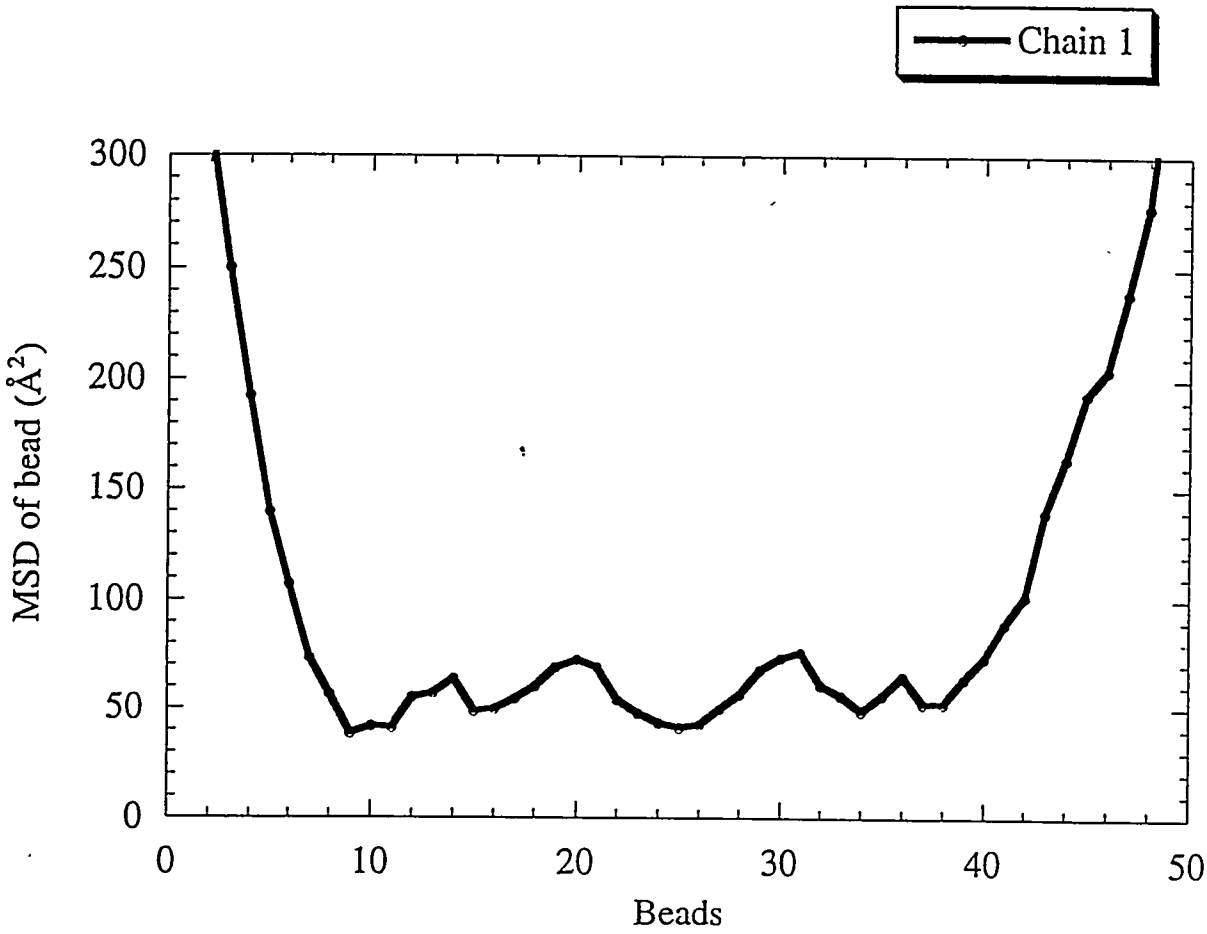
Chain 1
MSD of bead (Å²)
300
250
200
150
100
50
0
0
10
20
30
40
50
Beads

fig 17